2020-21 AIAA Design, Build, Fly Design Report

Illinois Institute of Technology

Contents

Acronyms, Initialisms, and Symbols

α	Aircraft angle of attack [deg]
ρ	Air density [slug/in.^{3}]
ω_d	Damped frequency [rad/s, Hz]
ω_n	Natural frequency [rad/s, Hz]
ζ	Damping ratio [–]
AIAA	American Institute of Aeronautics and Astronautics
AR	Aspect ratio [–]
b	Wingspan [in, ft]
c	Wing chord [in]
C_d, C_D	Drag coefficient (2D, 3D) [–]
C_{D0}	Zero-lift drag coefficient
C_f	Skin friction coefficient
C_{HT}	Horizontal tail coefficient [–]
C_l, C_L	Lift coefficient (2D, 3D) [–]
$C_{L_{\text{max}}}$	Maximum lift coefficient [–]
C_m, C_M	Moment coefficient (2D, 3D) [–]
C_{VT}	Vertical tail coefficient [–]
CA	Cyanoacrylate adhesive
CAD	Computational Aided Design
CFD	Computational fluid dynamics
CG	Center of gravity [in]
CNC	Computer numerical controlled
D	Drag
DBF	Design, Build, Fly
e	Oswald efficiency
ESC	Electronic speed controller
g	acceleration of gravity
GM	Ground mission score
IC	Integrated Circuit
IIT	Illinois Institute of Technology
LE	Leading Edge
LED	Light Emitting Diode
L	Lift
L/D	Lift-to-drag ratio [–]
L_S	Sensor pod length [in]
LiPo	Lithium polymer
M_1	Mission 1 score
M_2	Mission 2 score
M_3	Mission 3 score
N_{con}	Number of shipping containers
NiCd	Nickel-cadmium
NiMH	Nickel-metal hydride
RC	Remote-Controlled
Re	Reynold's number
S	Wing area [in.^{2}, ft.^{2}]
S_wet	Wetted area
TE	Trailing Edge
θ	Theta
T/W	Thrust-to-weight ratio [–]
UAV	Unmanned aerial vehicle
W/S	Wing loading [–]
W_S	Sensor pod weight [oz., lbf.]
v	Velocity [ft/s]
Wh	Watt-hours

1 Executive Summary

This report serves to outline the design, manufacturing, and testing processes of Illinois Institute of Technology's (IIT) 2020-21 Design, Build, Fly (DBF) team. The team's objective was to design, build, and test an unmanned aerial vehicle (UAV) with a deployable towed sensor pod. The maximum wingspan is 5 ft and the aircraft must take off within 100 ft.

Mission requirements dictate that the aircraft must transport a sensor pod and pod simulators stowed in shipping containers. When in flight, a sensor must be deployed, operated, and recovered while maintaining a fixed orientation and without impacting aircraft stability. The sensor must be at least 1 in. diameter and have a minimum length to diameter ratio of 4. In addition, the sensor functionality is defined by a minimum of 3 external lights that must be visible while in flight and each light must operate one at a time. These lights must be remotely controlled via a transmitter. The sensor must be deployed by a factor of ten times the length of the sensor from the exit of the aircraft. The sensor must be housed in a shipping container and fully enclosed to protect it from impact on a fall of 10 in.

The UAV must be capable of completing 3 missions and a ground mission as described in Table 3.1. Mission 1 requires 3 laps in 5 minutes with no payload. Mission 2 requires 3 laps in 5 minutes while carrying the sensor in its shipping container to simulate the deployment system. Mission 3 requires sensor deployment with as many 360° turns as possible in 10 minutes. The sensor must be recovered prior to landing.

Score analysis was conducted applying numerical preferences in chronological order, with 1 being the lowest and the maximum value being the highest preference.

The team was structured to guarantee work was divided appropriately and to ensure the team was successful in this year's contest. Meetings were held online due to campus regulations restricting in-person meetings to follow social distancing guidelines established by Illinois state policy. A more in-depth overview of the team's structure is discussed in Section 2. Following this, Section 3 discusses the approach used to develop a design and the individual sub-teams' methods.

A conventional single fuselage, high wing, monoplane with a conventional tail was selected during the early design stage due to its ease of manufacturing and payload capacity which is further described in Section 4. The final design plans are covered in Section 5. The aircraft will be constructed using balsa and heat shrink, expanded on in Section 6. Finally the aircraft will go through a testing regime defined in Section 7 and results will be discussed on Section 8.

2 Management Summary

The 2020-21, Illinois Institute of Technology (IIT) DBF Team consists of 10 members who are all full time students. Of these 10, three are seniors and the remaining seven are juniors or younger. Two of the underclassmen have previous experience in last year's contest.

2.1 Team Organization

The team is student led and consists of three subteams acting as separate entities for part of the design process. A faculty advisor was consulted for constructive criticism and an alternative perspective; he was chosen due to his experience building and flying Remote-Controlled (RC) planes. Students were organized in a chain of command. A student with strengths in organization is the Project Manager. A student with

previous technical qualifications is the Lead Engineer. The Lead Engineer advised the Project Manager throughout project development. All leadership roles are held by students with previous experience in Design, Build, Fly.

The Project Manager's primary responsibilities consist of keeping track of progress, delegating tasks, overseeing communications, and providing assistance where needed. The Lead Engineer's primary responsibilities consist of providing specific design constraints, time projections per task, and requesting specific administrative assistance throughout project phases. Assignments were delegated to all members, regardless of experience or ranking, to encourage participation, and foster an educational experience for all team members. Three subteams, consisting of Aerodynamics, Propulsion, and Structures are led by senior and junior students with expertise and experience in their respective fields. These branches provided a means for members to gain and utilize knowledge on a particular area of design. Majority of tasks were done collaboratively with subteams handling specifics related to their branch. The hierarchy of the team is shown in Figure 2.1.

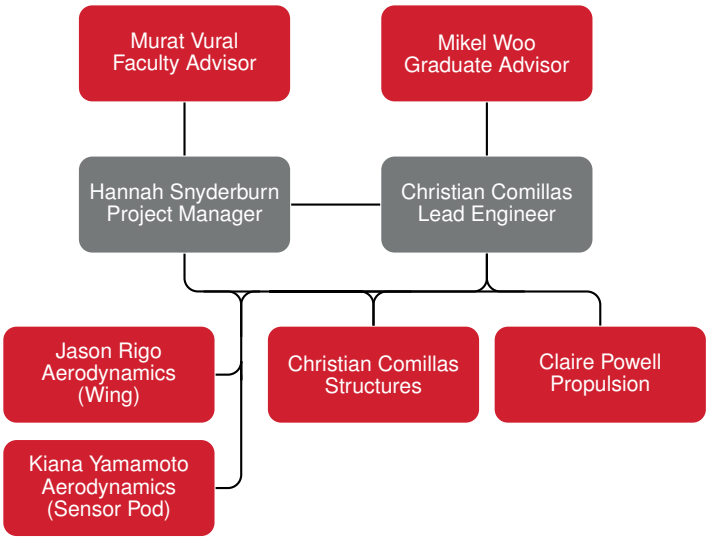

Figure 2.1 – Team Structure and Leaders

2.2 Milestone Chart

A milestone chart was developed shortly after publication of the contest rules. Its purpose was to ensure that the project will be completed on time and ensure tasks were delegated optimally. The Project Manager, Lead Engineer, and subteam leads were responsible for monitoring progress and informing the project manager whenever plans needed adjustment to ensure deadlines were met. An up-to-date chart is shown below in Figure 2.2.

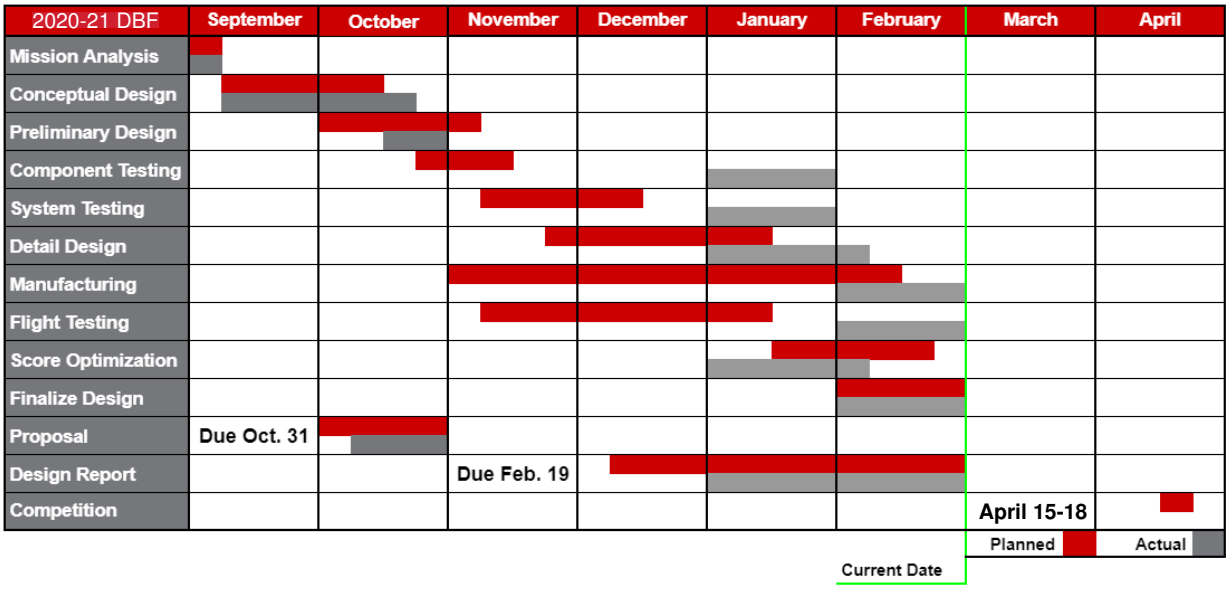

Figure 2.2 – Milestone Chart

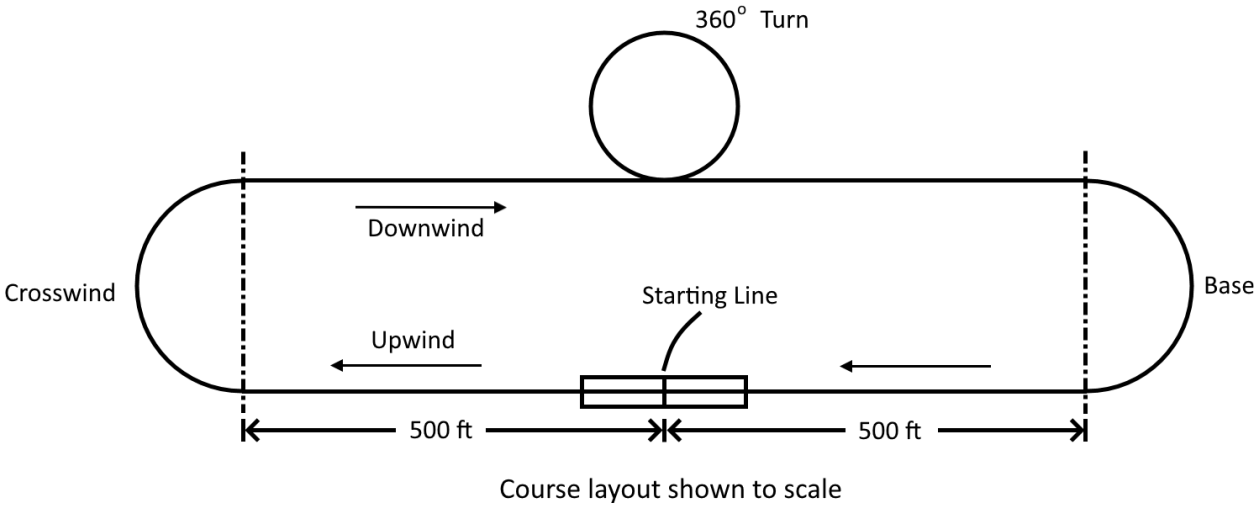

Figure 3.1 – Schematic of Course Layout. Adapted from [1]

3 Conceptual Design

The conceptual design stage of the aircraft utilized contest scoring and design restrictions to optimize design parameters. These parameters were used to compare various aircraft configurations to select the highest scoring configuration. Section 3.4 presents the final configuration selected.

3.1 Mission Requirements

AIAA's 2020-21 DBF rules specify that a UAV must be designed with the capability to transport, deploy/recover, and operate a towed sensor pod. This sensor pod must have a minimum cross sectional diameter of 1 in. and minimum length to diameter ratio of 4. Additionally, operation of the sensor pod requires the use of 3 external lights that must be activated remotely and operate in a pattern when deployed. The contest consists of three flight missions and a ground mission that can be attempted any time during the contest. Flight missions must be completed in order with one additional attempt allowed for missions 2, 3, and the ground mission to improve score.

Each flight mission consists of flying laps around the course depicted in Figure 3.1. Missions start when the throttle is first advanced. The aircraft must then takeoff within 100 ft of the starting line and then fly four legs: upwind, crosswind, downwind, and base. The upwind and downwind legs are both 1,000 ft long and centered about the starting line. The crosswind and base legs are both 180° turns. There is also a 360° turn at the midfield downwind position that must be completed. A lap ends when the aircraft passes over the starting line on the upwind leg. Finally, when the mission ends the aircraft must perform a successful landing (landing within runway bounds with no significant damage) for the mission to be scored. Before each flight mission the flight crew has 5 minutes to load and secure the payload.

Table 3.1 – Mission Summary and Scoring

Mission	Summary	Scoring
Staging Flight	No payload, 100 ft takeoff length, complete 3 laps in 5 minutes	$M_1 = 1.0$ (Successful landing)
Delivery Flight	Sensor in shipping container, shipping container simulators, deploy/recovery mechanism, 100 ft takeoff length, 3 laps in 5 minutes	$M_2 = 1 + \frac{\left(N_{\text{con}}/T_{M_2}\right)_{\text{IIT}}}{\left(N_{\text{con}}/T_{M_2}\right)_{\text{max}}}$
Sensor Flight	Sensor, deploy/recovery mechanism, 100 ft takeoff length, deploy sensor before first 360° turn, recover sensor after last 360° turn, complete as many laps as possible in 10 minutes	$M_3 = 2 + \frac{\left(N_{\text{laps}} \times L_S \times W_S\right)_{\text{IIT}}}{\left(N_{\text{laps}} \times L_S \times W_S\right)_{\text{max}}}$
Ground Mission	Drop sensor pod in shipping container from 10 in. on all sides and verify still operational, load all shipping containers, install deploy/recovery mechanism and sensor pod, deploy sensor pod	$GM = \frac{(T_{GM})_{\text{min}}}{(T_{GM})_{\text{IIT}}}$

3.1.1 Scoring Summary

Contest scoring is based on the below equation:

$$\textit{Score} = \textit{Written Report Score} \times \textit{Total Mission Score} \tag{3.1}$$

The overall score depends entirely on the quality of this report (*Written Report Score*) and the combined scores of all missions (*Total Mission Score*). *Total Mission Score* is simply the addition of all mission scores as follows:

$$\textit{Total Mission Score} = M_1 + M_2 + M_3 + GM \tag{3.2}$$

Values of M_1, M_2, M_3, and GM are given in Table 3.1. Additionally, the table presents a brief overview of each mission.

Mission 1: Staging Flight

This first mission does not require a payload and serves as a demonstration of the aircraft's stability and ability to fly in a controlled manner. No payload is carried. Three laps must be completed within a 5 min window starting when the throttle is advanced for the first time and ending when passing over the starting line on the final lap. Additionally, the aircraft must takeoff within 100 ft. Scoring for this mission is either a 1.0 (successful attempt) or a 0.0 (unsuccessful attempt).

Mission 2: Delivery Flight

Mission 2 serves to demonstrate the aircraft's ability to transport the sensor pods. The payload for this mission is the sensor in its shipping container, shipping container simulators, and the deploy/recovery mechanism. The minimum payload is the sensor in its shipping container and the maximum is the maximum number of shipping containers specified at tech inspection. The aircraft must complete three laps in a 5 min. window under the same conditions as Mission 1. Scoring is based upon the ratio of containers carried to time of completion compared to that of the highest score on Mission 2.

Mission 3: Sensor Flight

The final flight mission demonstrates the ability to deploy, operate, and recover the sensor pod as well as its affect on the UAV's endurance capabilities. The primary goal is to complete as many laps as possible within a 10 min. window using the specifications of the other flight missions. Upon takeoff the sensor pod must be fully deployed before the first 360° and fully recovered after the last 360° turn but before landing. While deployed, the sensor must be operated by having three lights that light up in a easily recognizable pattern that is visible from the ground. This pattern must be activated remotely from the ground via a connection from the aircraft. Finally, the sensor must have a section where the cross-section is constant with a minimum diameter of 1 in. and length to diameter ratio of 4. Finally, the sensor must be deployed at least 10 times the length of the constant cross-section region. The score on this mission is based on the product of laps completed, sensor length, and sensor weight compared to that of the highest Mission 3 score.

Ground Mission: Operational Demonstration

The ground mission's objective is to demonstrate the shipping container integrity, shipping container loading, and the deploy/recovery mechanism. An assembly crew member will drop the shipping container, with the sensor pod inside, from 10 in. on all sides before removing it and verifying that the sensor pod is not damaged and operates normally. After this, the assembly crew member will be timed on their ability to load the maximum Mission 2. They must remove the shipping containers and install the deployment/recovery mechanism and sensor pod at which point the timer will stop. Finally, the sensor pod will be partially deployed and then recovered to verify its operation. Scoring on the ground mission is the ratio of the fastest time to IIT's time.

3.2 Design Requirements

From the mission specification, relevant design parameters were chosen. A configuration was selected utilizing an approach that maximizes total mission score through analysis of the scoring parameters with the greatest impact.

3.2.1 Aircraft and Payload Constraints

While mission requirements constrain the design, it is further bounded by constraints imposed by the rules. Below are the restrictions put in place on the various components of the aircraft.

Aircraft Configuration

- 55 lbf weight limit
- 5 ft. maximum wingspan
- Shipping containers must be secured to prevent significant movement

Sensor Pod

- Minimum 1 in. diameter
- Minimum length to diameter ratio of 4
- Aerodynamically stable when deploying, operating, and recovering
- Minimum of 3 external lights visible from the ground
- Only one light at a time may be on and must display a pattern that is activated by the pilot
- Activation of the lights must be done via a physical connection to the aircraft
- Contain its own power supply compliant with the battery requirements
- Carried completely internal to aircraft

Shipping Container

- Fully enclose the sensor pod
- Protect sensor pod from drops
- Simulator dimensions must be within $\pm$1/8 in. of one another
- Simulators must weigh the same or more than the sensor and shipping container

Deploy and Recovery Mechanism

- Mounted completely internal to aircraft
- Deploy sensor 10 times the sensor length

Propulsion System

- Commercially available electric motors and propellers
- External switch to activate radio control system
- Cannot exceed 200 Wh.
- Nickel-cadmium (NiCd), nickel-metal hydride (NiMH), or lithium polymer (LiPo) batteries only
  - NiCd and NiMH
    - Only commercially available packs or individual cells
  - LiPo
    - Unaltered, commercially available
    - May not exceed 100 Wh. per pack
    - Fuse near positive terminal
    - If using multiple packs they must be identical, connected in parallel, and have a 0.25 in. gap between each battery
- One battery type

3.2.2 Score Sensitivity Analysis

An in-depth analysis of the scoring equations (see Table 3.1) was performed to identify how each design parameter affected the total mission score. Selection of these parameters was crucial to determining the most appropriate configuration. Design parameters were chosen such that they would directly relate to terms in the scoring equations.Table 3.2 outlines the chosen design parameters and their corresponding score terms.

Table 3.2 – Design Parameters

Parameter	Score Term	Objective
W/S	N_{con}, W_S	Increase the amount of weight that can be carried by the aircraft
C_L	N_{laps}	Minimize lap time while towing the sensor
T/W	T_{M_2}, N_{laps}	Complete laps as fast as possible with maximum payload

Wing loading (W/S) was selected for its direct relation to the amount of payload that can be carried and wing size. Lift coefficient (C_L) can be rewritten in terms of wing loading and velocity as so (assuming steady, unaccelerated flight):

$$C_L = \frac{2 \cdot L}{\rho v^2 S} = \frac{2 \cdot W/S}{\rho v^2} \tag{3.3}$$

Since velocity is inversely proportional to lap time, wing loading can now be related to mission time as well as airfoil selection. Finally, thrust-to-weight ratio (T/W) was selected as it relates to lap times and aids in

propulsion system selection. With these characteristics, aircraft parameters are now related to score terms.

Maximizing score was done by selecting baseline values for each parameter and then varying each parameter while holding the others constant. The design parameters were related to score thus changes in design parameters could be related to changes in total mission score. For the denominators associated with maximum scores, estimated extremes were used to get a conservative score estimate. Each design parameter change resulted in a new cruise velocity for each mission. The velocity was then used to determine T_{M2} and N_{laps} for calculating scores for Missions 2 and 3. Additionally, only design parameter values that were able to complete Mission 1 were considered in the analysis. Lap distance took into consideration each cruise velocity by calculating turn radius. Thus, extremely high cruise velocities would result in large turn radii. Results of this analysis are shown in Figure 3.2.

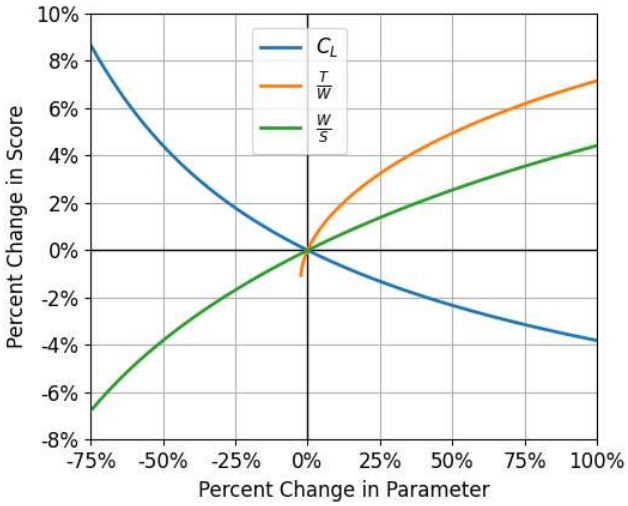

Figure 3.2 – Score Sensitivity Analysis

These results indicate that wing loading should be maximized since number of shipping containers is proportional to score. Score analysis showed lift coefficient should be minimized and velocity should be maximized to maximize score. Finally, a high thrust to weight ratio is desired to achieve the high velocity desired. Individual mission contributions to final score were also analyzed and showed that approximately 60% of total mission score comes from Mission 3. Therefore, sensor weight and length should be maximized and the number of containers would be based on the payload capabilities of the aircraft.

3.3 Configuration Selection

With score sensitivity analysis in mind, configuration selection was done by comparing various component options and selecting those which best represented the design parameter trends. The general process utilized a scoring system in which different configurations were ranked based on their relative superiority in various categories. Configurations were ranked from 1 (lowest) to N (highest), where N is the number of configurations considered. Each configuration's rank in every category was then multiplied by a predetermined weight and summed. The configuration with the highest total score was then selected.

3.3.1 Wing Configuration

Since it was preferred to maximize wing loading, lift was chosen as the most important criteria. Weight, payload capacity, and drag were all of equal importance to overall aircraft performance. Finally, stability

and ease of manufacturing were least important. Five different wing configurations were considered. The advantages and disadvantages are outlined below with a summary shown in Table 3.3.

Monoplane: The monoplane scored high on payload capacity, stability, and ease of manufacturing. In addition, its low weight and average drag were preferable.

Biplane: The biplane has high lift and an acceptable payload capacity. Its heavy weight, sub-par drag, stability, and difficult manufacturing were not a preferable option.

Tandem Wing: Tandem wing scored well in drag and stability while having below average scores in weight, lift, ease of manufacturing, and drag.

Blended Body: The blended body configuration scored well in lift and ease of manufacturing, but poorly in weight, drag, and stability. Payload capacity had an average score.

Flying Wing: A flying wing has low payload capacity and poor stability. Low weight and low drag were positive traits taken into consideration.

Table 3.3 – Wing Configuration Selection Matrix

Criteria	Weight	Monoplane	Biplane	Tandem Wing	Blended Body	Flying Wing
Lift	25	1	5	2	4	3
Weight	20	4	2	3	1	5
Payload Capacity	20	5	4	2	3	1
Drag	20	3	1	4	2	5
Stability	10	5	3	4	2	1
Ease of Manufacture	5	5	3	1	4	2
Total	100	340	310	275	260	315

3.3.2 Wing Location

Placement of the wing contributes to several effects that are important to all stages of flight. First, and most importantly, wing placement will have a significant impact on stability. Different wing locations will also enable various landing gear configurations to be considered. Ground effect will have a significant impact on low altitude performance–particularly with takeoff and landing distance. Different structural geometries will be required for each placement and affect the difficulty of manufacturing. Three different wing locations were considered. The advantages and disadvantages are outlined below and summarized in Table 3.4.

Low Wing: The low wing location would be the least stable while having the best ground effect and ease of landing gear placement.

Mid Wing: Having a mid wing setting has overall median scores in stability, ground effect, landing gear placement. It is the most difficult to manufacture.

High Wing: The high wing placement would lead to the best stability and ease of manufacturing. It has the most difficult landing gear placement and poor ground effect.

Table 3.4 – Wing Location Matrix

Criteria	Weight	Low Wing	Mid Wing	High Wing
Stability	50	1	2	3
Landing Gear	20	3	2	1
Ground Effect	15	3	2	1
Ease of Manufacture	15	2	1	3
Total	100	185	185	230

3.3.3 Motor Configuration

Single and twin motor configurations were considered. They were rated on their weight, stability, thrust, and complexity. Weight and stability were equally important. A lower weight would allow for more payload while twin motors have no P-factor to counteract. With no P-factor, the vertical stabilizer could be smaller thus reducing weight. Thrust was important because higher thrust means a higher payload. Finally, complexity was considered for the extra electronics and layout planning required. The advantages and disadvantages of each configuration are discussed below and summarized in Table 3.5.

Single: A single motor would be the lightest and least complex option.

Double: Double motors ranked high in thrust and stability. Its disadvantages include their high weight and complexity.

Table 3.5 – Motor Configuration Matrix

Criteria	Weight	Single	Double
Weight	30	2	1
Stability	30	1	2
Thrust	25	1	2
Complexity	15	2	1
Total	100	145	155

3.3.4 Fuselage Configuration

Since a twin motor configuration was selected, the possibility of a twin fuselage design was made available. Primary factors for a fuselage were aerodynamic forces and structure. The number of fuselages will affect the amount of lift generating wing area and amount of structural material to build. Lift and weight were the primary factors in the decision. Equally important was the amount of internal volume because more volume meant longer sensor pods could be used. Drag is a major consideration when increasing the size of any component. Finally, difficulty involved with manufacturing was a consideration. Outlined below are the advantages and disadvantages of each with a summary presented in Table 3.6.

Single Fuselage: The single fuselage had superior lift, lower weight and drag. It was also the easiest to manufacture. It had the least payload capacity and is the least stable fuselage.

Twin Fuselage: The twin fuselage had the greatest payload capacity and stability while scoring the worst with lift, weight, drag, and manufacturing ease.

Table 3.6 – Fuselage Selection Matrix

Criteria	Weight	Single Fuselage	Twin-Fuselage
Lift	25	2	1
Weight	20	2	1
Payload Capacity	20	1	2
Drag	20	2	1
Stability	10	1	2
Ease of Manufacture	5	2	1
Total	100	170	130

3.3.5 Tail Configuration

The tail of the aircraft presents several design considerations that will have a major impact on aircraft performance. Most important were the structural integrity and stability provided by the configuration. Additionally, it was nearly as important to have a configuration that allowed for appropriate control authority. Again weight was a point of consideration. A rather unique criterion was the configuration's expected behavior at higher angles of attack which is particularly important during takeoff, landing, and gusting conditions. Ease of manufacturing was a point of concern. Five different tail configurations were considered. The advantages and disadvantages are outlined below and summarized in Table 3.7.

Conventional: A conventional tail provides excellent stability and control, while allowing for light weight construction and ease of manufacturing. Possible issues with downwash from the wing affecting control surfaces.

T-Tail: An advantages of the T-tail is keeping the elevators out of the disturbed airflow from the wing and fuselage. This also allows for improved glide ratio. However, due to the elevator being above the vertical stabilizer, this requires the stabilizer to be stronger, leading to increase weight due to the added support. The T-tail scored well for controls but scored average or below average for all other factors.

H-Tail: An H-tail allows for the vertical stabilizer to be free from the parasitic drag produced by the fuselage and has reduced stress at the root. The two vertical stabilizers cause a heavier and stronger root, causing manufacturing and design complications. H-tail scored well in AOA performance, rigidity, stability, and weight, while scoring low in controls and ease of manufacturing.

Boom Mounted: An advantage of a boom mounted tail is that it allows for a large payload capacity due to the separation of the tails and would be easier to deploy and retract the sensor pod. Disadvantages include the drastic increase in weight and drag due to boom design. Having the elevator between the two vertical stabilizers would be less effective than a conventional design due to the disturbed airflow from the fuselage.

Ring Tail: The major advantage of the ring tail is stability due to a large surface area to control both vertical and horizontal axes. A disadvantage is the drag, difficulty of manufacturing, and the complexity of implementation and design of a ring tail.

Table 3.7 – Tail Configuration Matrix

Criteria	Weight	Conventional	T-Tail	H-Tail	Boom-Mounted	Ring-Tail
Rigidity	30	5	2	4	3	1
Stability	25	5	2	4	1	3
Controls	20	5	4	2	1	3
Weight	10	5	3	4	1	2
AOA Performance	10	4	1	5	2	3
Ease of Manufacture	5	5	2	3	4	1
Total	100	490	240	365	185	220

3.3.6 Landing Gear Configuration

The advantages and disadvantages are outlined below and summarized in Table 3.8.

Tricycle: The Tricycle landing gear was selected due to its superior handling capacity as well as anticipating sensor deployment/recovery operations while remaining cognizant of the need for ease of manufacturing. This landing gear was determined to be straightforward in assembly, despite its lower drag and higher weight disadvantages.

Tail-Dragger: The conventional landing gear scored best with its low drag capabilities and light weight. It produces less parasitic drag due to its placement further from the center of gravity, which supports a smaller portion of the overall aircraft weight and resulting in its capacity to be made smaller and lighter.

The Tail-Dragger is most susceptible to ”nose-over” and thus scored low in handling capabilities. The sensor’s deployment/recovery were considered in configuration determination and was predicted to be hindered by a conventional landing gear as well as being more complex to manufacture.

Table 3.8 – Landing Gear Configuration Matrix

Criteria	Weight	Tricycle	Tail-Dragger
Handling Characteristics	30	2	1
Deployment Reliability	25	2	1
Ease of Manufacturing	20	2	1
Drag	15	1	2
Weight	10	1	2
Total	100	175	125

3.4 Final Conceptual Design

The final design will be a high-wing, conventional monoplane with two wing-mounted motors. This configuration ensures that the aircraft will have high speed and payload capacity. Additionally, it will be easier to make the aircraft stable and have acceptable low-speed performance. Manufacturing should be relatively easy–which is quite beneficial for following COVID-19 health precautions.

4 Preliminary Design

Having selected a configuration, the preliminary design phase aimed to narrow down the design parameters to a range where maximum score could be achieved. Focus was placed primarily on maximizing the score for Mission 3 since it contributed the most to the total mission score. For this, it was desired to maximize

sensor weight and lap time. Mission 2 scoring would then be used to determine sensor length based on payload capacity and internal volume of the aircraft. Trade studies, software analysis, and numerical solvers were utilized to appropriately size and compare the performance of various configurations.

4.1 Design Methodology

Preliminary design was done through an iterative process where feedback from subteams was used to modify design elements. Each subteam had several key components that were the crux of this design phase. Below is a summary of each subteam's requirements and objectives for component design.

4.1.1 Aerodynamics

Due to the need for a low C_L but high wing loading design, airfoil selection and wing geometry aimed to maximize the lift-to-drag ratio (L/D). A high L/D would provide the necessary payload capacity while allowing for high cruise velocities. L/D is limited by the wing's aspect ratio (AR) due to the 5 ft. wingspan limitation. Additionally, the aircraft must demonstrate exceptional handling and stability qualities to cope with the heavy sensor pod being towed at such a far distance behind the aircraft.

4.1.2 Structures

The wing structure utilizes a central spar and ribs. The spars receive stress from the ribs. The ribs take load from the skin of the wings. Components will be designed using computer aided design (CAD).

The fuselage was composed of a truss structure, designed to provide the overall structural support of the aircraft while carrying the payload. The truss was selected to ensure stiffness in the longitudinal direction was possible to withstand longitudinal bending, to withstand weight and lift from the tail in the form of bending moments and torsional loading from the fin and rudder. The longerons were built to compose an entire length of the overall structure. A monocoque structure was considered but the truss was preferred due to its exceptional manufacturing simplicity.

4.1.3 Propulsion

The battery, motor, and propeller were selected to meet thrust demands while recognizing the weight consideration for score analysis advantage. Static thrust was important particularly for Mission 2, which required carrying the sensor pod and shipping container payloads. The ideal combination would result in a shorter Mission 3 lap time to improve score. A battery and motor combination was selected based upon its ability to meet a desired cruise speed (41 mph,) and flight time (over 10 minutes.).

4.1.4 Payload

The sensor pod, its shipping container, and the deployment and recovery mechanism must fit inside of the fuselage while following the sizing ratios as regulated by AIAA. The sensor pod weight was maximized for score analysis. The sensor pod was designed to house the onboard LED circuit required for Mission 3, shown in Figure 5.7.

4.2 Design Trade Studies

4.2.1 Wing Sizing

Selection of wing geometry began by considering how the highest L/D could be achieved. From classical wing analysis it was know that an elliptic wing with a constant airfoil and no twist has the highest theo-

retical L/D. Therefore, the primary objective for the wing design was to achieve an elliptic lift distribution. Constructing a pure elliptical wing posed both structural and analytic complications due to the complex geometry of such a wing. At least two of the following three actions needed to be done to overcome these complications: change wing planform, change the airfoil, and/or add twist. Of the three options, twist would be the most difficult to manufacture and design structurally. An elliptic lift distribution needed to be achieved by various airfoil selections determined by the wing planform. To determine the optimal AR and wing planform area (S), a trade study was performed. This process was done by estimating the maximum L/D for various AR and S combinations. The maximum lift to drag ratio can be estimated using the below equations from [3, 5, 6].

$$\left(\frac{L}{D}\right)_{\text{max}} = \frac{1}{2}\sqrt{\frac{\pi \varepsilon AR}{C_{D0}}} \tag{4.1}$$

$$C_{D0} = C_f \frac{S_{\text{wet}}}{S} \tag{4.2}$$

$$C_f = \frac{0.027}{Re^{1/7}} \tag{4.3}$$

Where:
ε = Oswald efficiency factor
C_{D0} = Zero-lift drag coefficient
C_f = Skin friction coefficient
S_{wet} = Wetted area
Re = Cruise Reynold's number

Several terms required for the above calculation needed to be estimated. The Oswald efficiency factor is how close a wing is to a theoretical elliptic wing and was assumed to be 1.0 as it is less critical for this analysis. S_{wet} is the total area exposed to the air. S_{wet} was found by assuming the aircraft consists of a rectangular fuselage and flat plate wing. These assumptions provided a sufficient estimate. Finally, a Reynold's number of 300,000 was used. Results of the analysis are shown in Figure 4.1. The darkened region shows where the wingspan is over 5 ft.; this region could not be considered. Where the current design falls within this region was also marked.

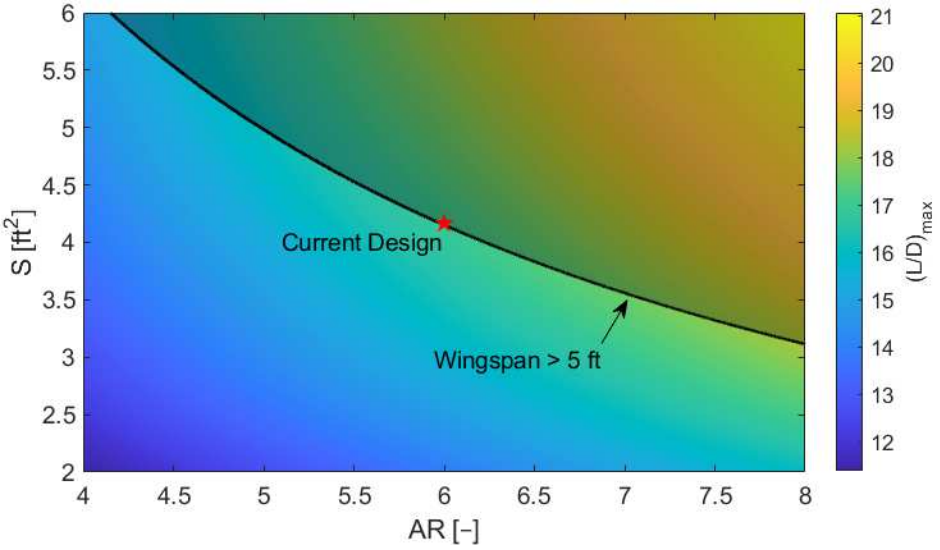

Figure 4.1 – Wing Sizing Trade Study

While the current design is not in the region with the highest possible L/D, it is relatively high at about 17. A lower wing area was not selected due to concerns with payload capacity and structural integrity. Thus, a wing area between 4.0 $ft.^2$ to 4.25 $ft.^2$ was chosen as it provided the best combination of payload capacity and structural integrity. A wing span of 5 ft. was chosen because maximum wing span was desired. The wing area was 600 $in.^2$. From this chosen wingspan and wing area the root chord was found from that of an ellipse. This would be the root chord of all wing geometries used to achieve an elliptic lift distribution. The root chord was found to be between 12.25 and 13.00 in. using the below equation.

$$S = \frac{\pi}{4} b c_r \;\rightarrow\; c_r = \frac{4S}{\pi b} \tag{4.4}$$

4.3 Sensor Pod Circuit

The circuit for the sensor pod is a sequential circuit designed from scratch utilizing a combination of 3 NAND gates and 3 D-Flip-Flops. The process began with a Finite State Machine diagram shown in Figure 4.2. Here each light combination is shown as a separate state and the inputs are a binary signal provided by the transmitter and receiver combination. A high signal, or 1, represents a lit LED. The input signal advances the lit LED state through a loop displaying a repeating pattern. No input signal returns it to a ready state flashing all lights on and off. This was done to visually identify if the sensor pod is powered. The diagram was then translated into into the truth table shown below in Table 4.1. Here the relation between the LED states and input signal can be seen as well as the required D-Flip-Flop signal input. These Flip-Flops were utilized to ensure the lighting pattern automatically cycles through each state.

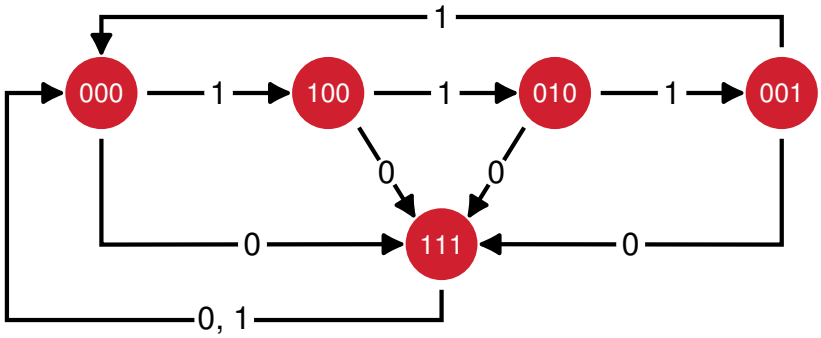

Figure 4.2 – Sensor Pod Finite State Machine Diagram

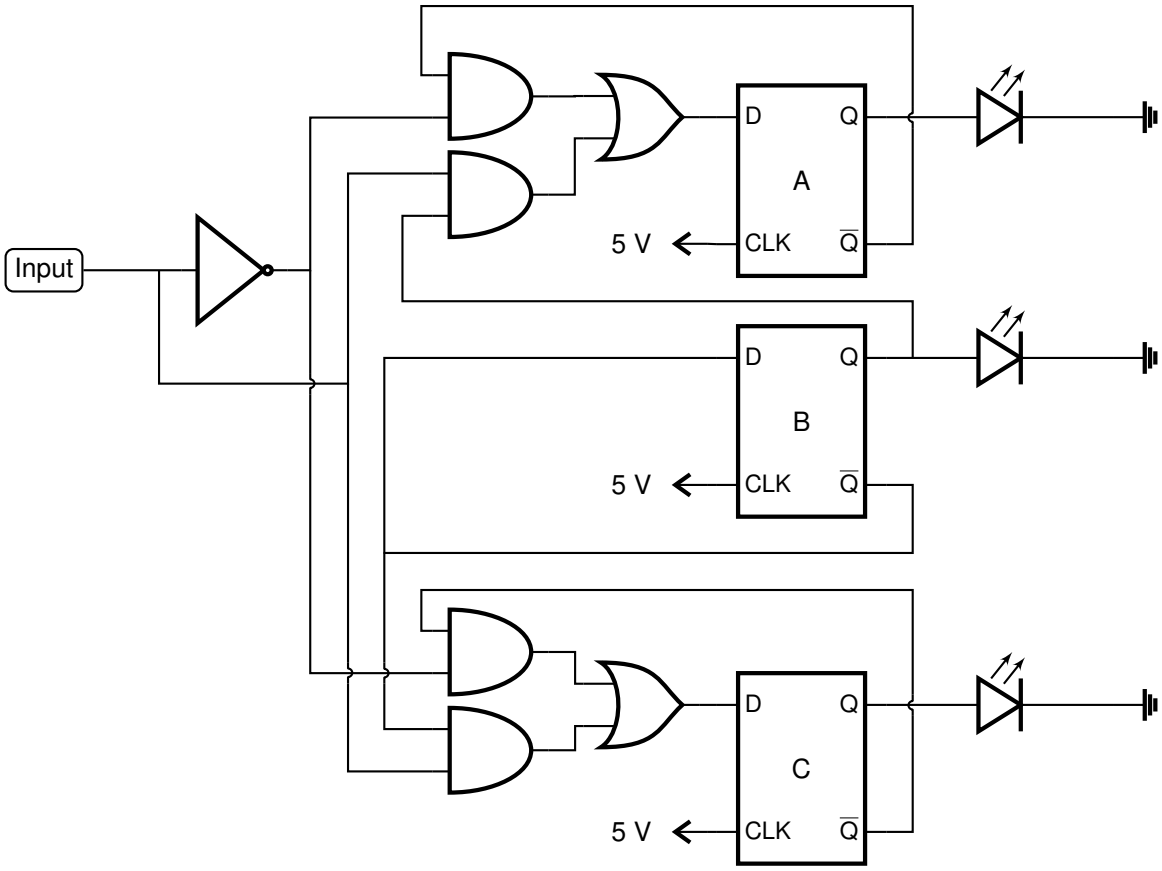

Figure 4.3 – Sensor Pod Circuit Diagram

Table 4.1 – Sensor Pod Truth Table

Present State			Input	Future State			D-Flip-Flop Inputs		
A	B	C	I	A	B	C	DA	DB	DC
0	0	0	0	1	1	1	1	1	1
0	0	0	1	1	0	0	1	1	1
0	0	1	0	1	1	1	1	1	0
0	0	1	1	1	0	0	1	1	1
0	1	0	0	1	1	1	1	0	1
0	1	0	1	0	0	1	1	1	1
0	1	1	0	x	x	x	x	x	x
0	1	1	1	x	x	x	x	x	x
1	0	0	0	1	1	1	0	1	1
1	0	0	1	0	1	0	1	1	1
1	0	1	0	x	x	x	x	x	x
1	0	1	1	x	x	x	x	x	x
1	1	0	0	x	x	x	x	x	x
1	1	0	1	x	x	x	x	x	x
1	1	1	0	x	x	x	x	x	x
1	1	1	1	x	x	x	x	x	x

Table 4.2 – Sensor Flip Flops

(a) D-Flip-Flop A

DA	CI			
AB	00	01	11	10
00	1	1	1	1
01	1	0	x	x
11	x	x	x	x
10	0	1	x	x

(b) D-Flip-Flop B

DB	CI			
AB	00	01	11	10
00	1	1	1	1
01	0	0	x	x
11	x	x	x	x
10	1	1	x	x

(c) D-Flip-Flop C

DC	CI			
AB	00	01	11	10
00	1	1	1	0
01	1	0	x	x
11	x	x	x	x
10	1	1	x	x

This table was then rearranged into Karnaugh maps, seen in Table 4.2 and simplified to find the simplest Boolean algebra function. Using these Karnaugh maps, the required Flip-Flop equations can be seen below.

$$Y = \bar{A}\bar{I} + \bar{B}I \tag{4.5}$$

$$Y = \bar{B} \tag{4.6}$$

$$Y = \bar{C}\bar{I} + \bar{B}I \tag{4.7}$$

4.4 Aerodynamics

Aerodynamic analysis was primarily performed using XFLR5–an XFOIL based software that predicts a wide array of aerodynamic properties of airfoils and wings. Additionally, it is capable of static and dynamic stability analysis. Several aerodynamic properties were of utmost importance when developing the design. Since an elliptic lift distribution was desired, developing a design required extra work. First, a wing geometry had to be selected to most easily achieve an elliptic lift distribution. The selected geometry would allow for optimal airfoil properties to be determined. The design of the sensor pod requires that it be aerodynamically stable. With the properties of the sensor pod determined, full stability analysis of the aircraft could be determined for every mission.

4.4.1 Wing Geometry

Selecting the wing geometry was done such that the wing most closely represented an elliptic planform. This would ensured that airfoil selection was simple. Three options were considered: trapezoid, swept trapezoid, and tapered. Figure 4.4 shows the reference elliptic planform and the other planforms considered. For each planform considered, the quarter chord is represented by the dotted line and a comparison against the reference planform is shown in red.

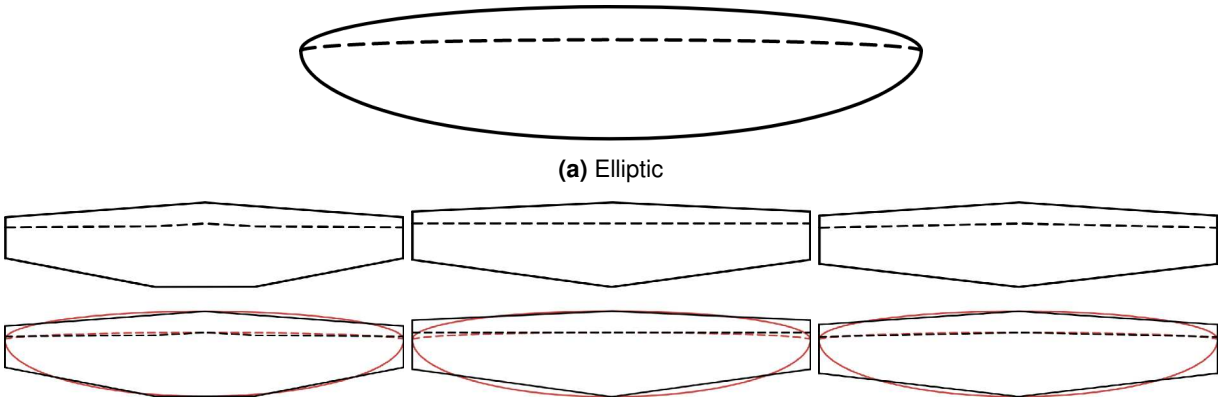

(a) Elliptic

(b) Tapered **(c)** Trapezoid **(d)** Swept Trapezoid

Figure 4.4 – Considered Wing Geometries

Table 4.3 – Reference Airfoil Comparison @ Re $= 300,000$

Airfoil	Max Camber [% chord]	Location [% chord]	Max Thickness [% chord]	Location [% chord]	$C_{l,\max}$ [–]	$(L/D)_{\max}$ [–]	$C_m(\alpha = 0)$ [–]
MH 113	6.4	47.7	14.7	29.7	1.79	102	-0.19
MH 114	6.4	50.0	13.0	28.1	1.76	108	-0.19
GOE 414	5.3	39.7	13.6	29.7	1.33	86	-0.12
GOE 422	6.5	39.5	17.1	29.5	1.66	82	-0.14
Root	6.2	42.4	9.3	24.7	1.49	105	-0.12
Tip	5.7	45.9	10.6	23.5	1.50	104	-0.13

The above geometries were selected for their close resemblance to the elliptic planform. The tapered planform shows the closest resemblance to the elliptic one, but several major issues were present with this planform. First, the strange quarter chord results in structural design difficulty and most likely a heavy wing. Furthermore, the strange chord variation would require complicated airfoil selection to ensure that the lift distribution does not have sharp gradient changes. Due to the difficulty associated with this planform, the trapezoid planform was chosen. Comparing the unswept to the swept version shows that the swept planform more closely represents the elliptic planform. Again, the swept quarter chord would have similar structural issues as the tapered, but significantly less so. Therefore the unswept trapezoid wing was chosen as it provides challenges without inducing too many design troubles.

4.4.2 Airfoil Selection

A trapezoidal planform requires that, at a minimum, the wing root and tip have different airfoil sections. Since there is no twist, the amount of lift produced by each wing section will be proportional to the chord length. Additionally, chord length changes linearly making airfoil selection slightly easier. In order to achieve an elliptic lift distribution from a linear change in airfoil, it was necessary for the tip airfoil to have a higher lift coefficient (C_l) than the root airfoil. This ensured that lift will decrease more slowly near the root and increase more rapidly near the tip, thus generating an elliptic lift distribution. However, if the difference was too large, then the distribution had a lift distribution resembling the number three or a triangular shape– both of which were undesirable. Through analysis of various airfoils in XFLR, it was determined that custom airfoils would be utilized. Custom airfoils would enable the team to not only achieve the desired aerodynamic properties but also ensure that the airfoil geometry would be structurally feasible. Design of the airfoils was

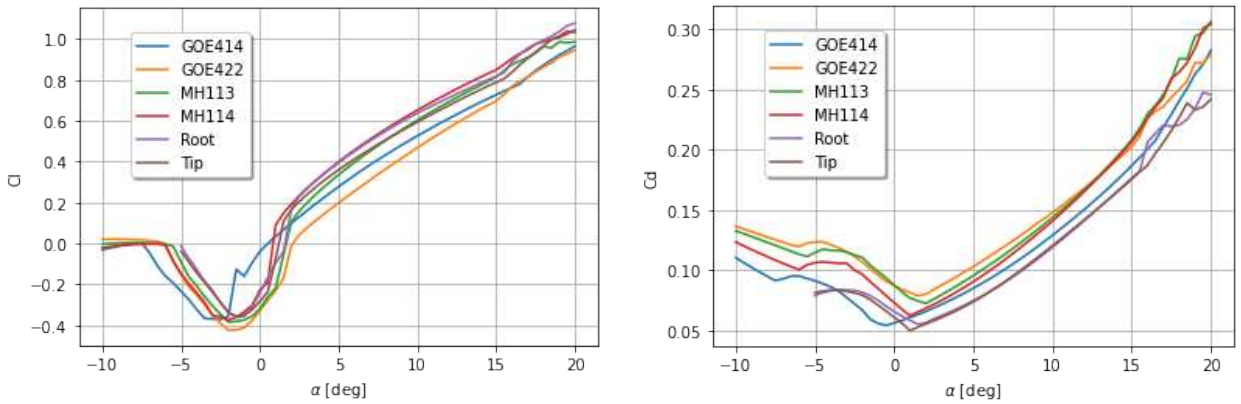

(a) C_l vs α **(b)** C_d vs α

Figure 4.5 – Airfoil Aerodynamic Properties @ Re $= 300,000$

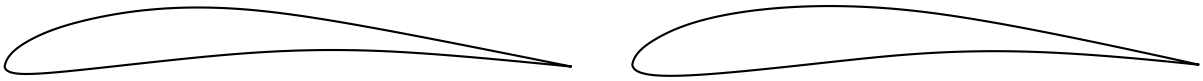

(a) Root **(b)** Tip

Figure 4.6 – Final Airfoil Designs

inspired by the MH 100 series mid-span propeller airfoils [2] and the Gottingen 400 series airfoils. These airfoils in general tend to provide high lift, low drag, and sufficient thickness ratios. This high lift is achieved by large camber, thickness, or both. Table 4.3 shows the pertinent airfoil properties for the reference airfoils and those that were designed. An important feature to note is that all of the reference airfoils have their maximum thickness aft of the quarter chord position. For structural reasons, the maximum thickness was desired to be as close to the quarter chord as possible. Next, it was observed that the airfoils have high lift, but varying L/D ratios. While the MH series airfoils have higher lift-to-drag ratios, their lift values were higher than desired per the score analysis. Thus the airfoil design focused on maximizing the lift-to-drag ratio while reducing the lift coefficient some. Finally, stability concerns were taken into account for the design. It was desired to have very low moment coefficient magnitudes. Knowing all of this, the lower surface and trailing edge resemble that of the MH airfoils and the upper surface had a similar camber line to the GOE airfoils. After several iterations the below designs (Figure 4.6) were found to exhibit the desired properties. The two airfoils were quite similar with only minor differences, and as shown on (Figure 4.5) the performance was very similar to other known airfoils. Most notably, the tip foil had a lower camber but higher thickness. These two properties effectively cancel each other out which results in a tip lift coefficient that was higher than the root's lift coefficient–as was desired. Table 4.3 shows that the maximum thickness was close to the quarter chord for both airfoils, allowing for a simpler main spar and lower structural weight. The tip thickness was increased to prevent the wingtip region from being fragile. As desired, the lift-to-drag ratio was similar to that of the MH airfoils, but the moment coefficient was similar to that of the GOE airfoils. There were also some secondary benefits that arose; primarily the gentle stall characteristics of both airfoils. Additionally, the straight trailing edge provides the option to make simple control surfaces using flat plates. Figure 4.7 shows the aerodynamic properties of the airfoils over a range of angle of attack. The airfoils were fairly similar to one another. An important aspect was the nearly linear slope of L/D at low angles of attack. This was due to a near constant drag coefficient at angles of attack from roughly $-3°$ to $8°$. Having such a wide

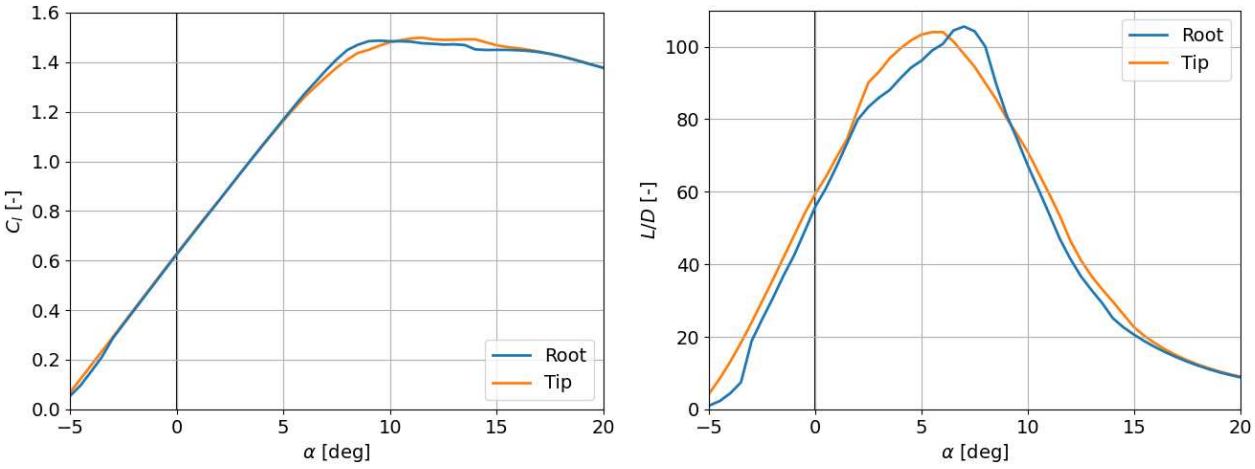

(a) C_l vs α **(b)** L/D vs α

Figure 4.7 – Airfoil Aerodynamic Properties @ Re $= 300,000$

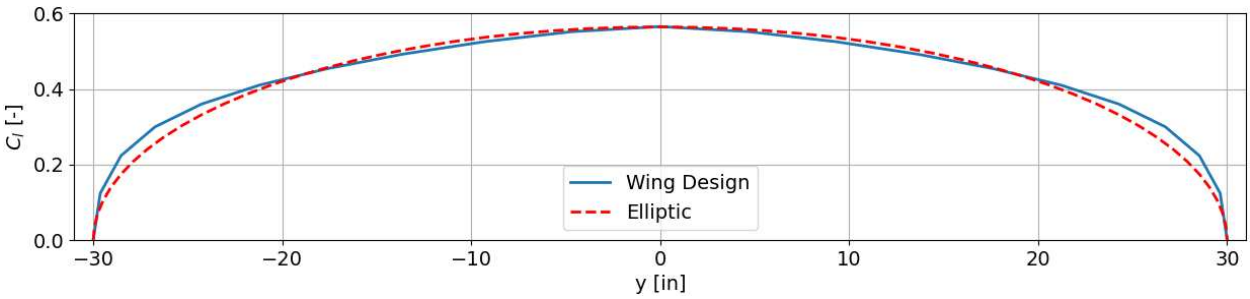

Figure 4.8 – Lift Distribution of Wing Compared to Elliptic Distribution

range where drag was constant was extremely useful. It ensured that the drag on the entire wing would remain relatively low in all phases of flight.

Finally, the lift distribution of the wing using these airfoils should closely match an ellipse. A wing area of 600 in^2 was chosen resulting in a root chord of 12.75 in. and tip chord of 7.25 in. Using these dimensions and the above airfoils, the wing generates the desired amount of lift and matches the elliptic profile quite well. Figure 4.8 shows the wing's lift distribution versus the elliptic distribution. The error between these two curves was 0.3%, which was a highly positive result.

4.4.3 Sensor Pod Sizing

A stabilization mechanism needed to be designed for the sensor pod in order to keep it aerodynamically stable while deployed, operated, and recovered as according to the contest rules. In order to meet this requirement, it was determined that fins should be placed on the sensor pod, as folding aerodynamic structures were prohibited. Determination of the sizing and placement of the fins began with the drawing of free body diagrams of the sensor pod for both the side and top of the pod (Figure 4.9). The force balance equations derived from these diagrams were put into a Python solver to determine the values of the tension, angle between the horizon and tow cable, and ratio between the displacement of the tow cable and the fins, all seen in Table 4.4. Fin planform area was parameterized and modified until a feasible angle and tension were found. Lift and drag values were computed using XFLR5 for each fin area. The drag on the sensor pod itself was estimated using experimental correlations presented in [4]. This methodology was used to reduce the number of unknowns to create a problem that could be solved analytically.

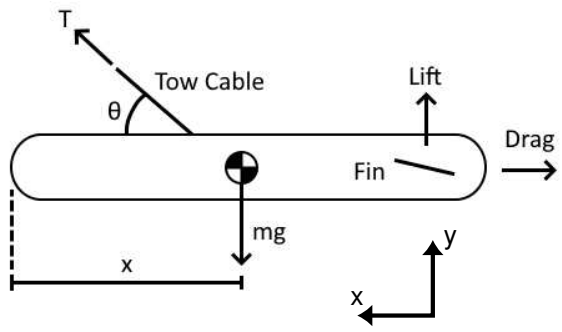

Figure 4.9 – Free body diagram of pod from side perspective

$$\sum F_x = T\cos(\theta) - D = 0 \tag{4.8}$$

$$\sum F_y = T\sin(\theta) + L - mg = 0 \tag{4.9}$$

$$\sum M_{cg} = T\sin(\theta)x_{cable} - Lx_{fin} = 0 \tag{4.10}$$

Where:
F_x = Force on x-axis
F_y = Force on y-axis
M_{cg} = Moment about the center of gravity
T = Tension in tow cable
mg = Weight of sensor pod
θ = Angle between horizon and tow cable
x_{cable} = Displacement of cable from CG
x_{fin} = Displacement of fin from CG

Table 4.4 – Fin Configuration Options from Solver

α_{fin} [deg]	Tension [lbf]	θ [deg]	x_{cable}/x_{fin} [–]
−5.0	2.71	23.2	−0.061
−2.0	2.69	22.3	−0.020
0.0	2.68	21.9	0.000
2.0	2.67	21.5	0.021
5.0	2.66	20.6	0.070

4.4.4 Stability

Static stability of the aircraft started with rough determination of vertical and horizontal stabilizer sizing using the method described in [5]. This was done by selecting a tail volume coefficient for both the horizontal and vertical stabilizers which were used to determine an appropriate stabilizer planform area. Equations 4.11 and 4.12 describe the tail coefficient equations.

$$C_{HT} = \frac{L_{HT} S_{HT}}{c_w S_w} \qquad (4.11) \qquad\qquad C_{VT} = \frac{L_{VT} S_{VT}}{b_w S_w} \qquad (4.12)$$

Both of these equations represent the ratio of the stabilizer effect to the wing geometry. The lengths (L_{HT} and L_{VT}) are the distance from the wing quarter chord to the tail quarter chord. Similarly, S_{HT} and S_{VT} are the planform area of the horizontal and vertical stabilizers, respectively. The denominator has the typical wing dimensions. For this aircraft, the following values were selected based on similarly sized aircraft: $C_{HT} = 0.5$ and $C_{VT} = 0.02$. In an effort to reduce structural weight, it was desired to have L_{HT} and L_{VT} less than or equal to 3 ft. With this length requirement, Equations 4.11 and 4.12 could be rearranged to solve for the required stabilizer areas. Doing this results in the following values: $S_{HT} = 85.42$ in^2 and $S_{VT} = 20.00$ in.^{2}. These areas were then used to iteratively select tail geometry until a satisfactory design was found. The final tail geometry resulted in high cruise velocities for Missions 2 and 3 as well as extremely high efficiencies and lift-to-drag ratios (see Table 4.5). In fact, the lift-to-drag ratio was just below the maximum value for each mission. The static margin for each mission was less than ideal, but this was expected with the short moment arm of the tail. The row for mission shows the range of values when the pod is stowed to when it is deployed.

With the aircraft statically stable it was also important to analyze the dynamic stability of the aircraft to ensure it could withstand gusts and other disturbances during flight. Longitudinal and lateral modes were analyzed using XFLR5 for each mission configuration. Figure 4.10 is the root locus of all five stability modes for each mission configuration.

Table 4.5 – Static Stability Cruise Properties

Mission	α [deg]	v [ft/s]	C_L [–]	e [–]	L/D [–]	Static Margin [%]
M_1	1.86	38.9	0.67	0.98	16.53	18.31
M_2	2.57	49.9	0.73	0.99	17.19	17.00
M_3	-0.162 to -0.294	47.6–53.5	0.49–0.54	0.92–0.99	2.97–17.67	5.45–24.66

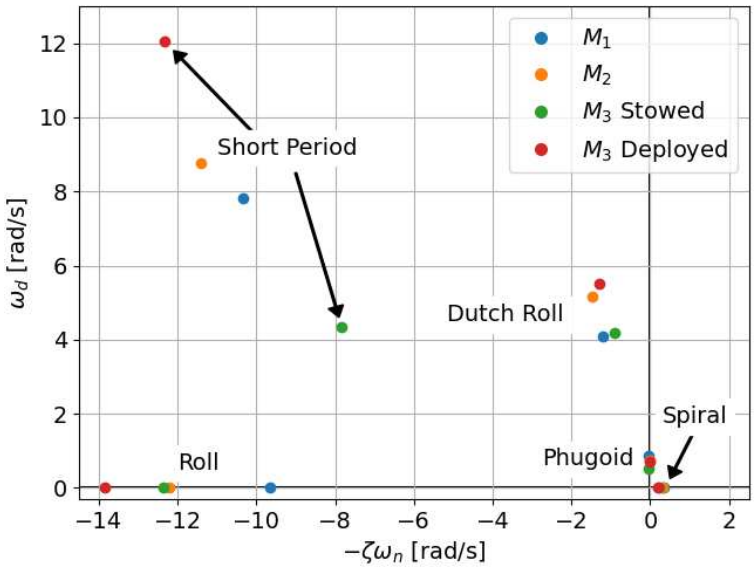

Figure 4.10 – Root Locus of Dynamic Stability Modes

All modes except spiral were stable for each mission configuration. Having the spiral mode unstable was acceptable given that its double amplitude time was around 2.0–2.5 s for each mission which can be easily corrected by the pilot. Similarly, the phugoid mode was nearly unstable for each mission but can also be easily corrected by the pilot as its half amplitude time was from 23–29 s. Both the short period and roll mode were highly stable with very short half amplitude times. Finally, the dutch roll mode was sufficiently damped with a half amplitude time of about half a second for each mission.

4.4.5 Winglet

Benefits of a winglet addition were considered to improve cruise efficiency. Flow around the wingtip was analyzed to determine an appropriate winglet geometry. The primary goal of the winglet design was to prevent the high pressure flow below the wing from spilling onto the low pressure upper surface. This would increase the local lift coefficient by reducing the downwash angle near the wingtip. Two major constraints were placed on the winglet geometry. First being that the wingspan could not change and the winglet could not exceed the wingspan limitation. The second limitation was that the geometry should not be complex or be exceedingly heavy. It was determined that a wingtip fence would be the best option to meet these criteria. Flow visualization was done using ANSYS Fluent–a computational fluid dynamics (CFD) program. After running the simulation for the wing, the streamlines in Figure 4.11a were analyzed to determine the regions where the wing fence would be most effective. From the diagram one can determine that the wingtip vortex forms near the half chord position and grows outward from there. Figure 4.12 shows the geometry

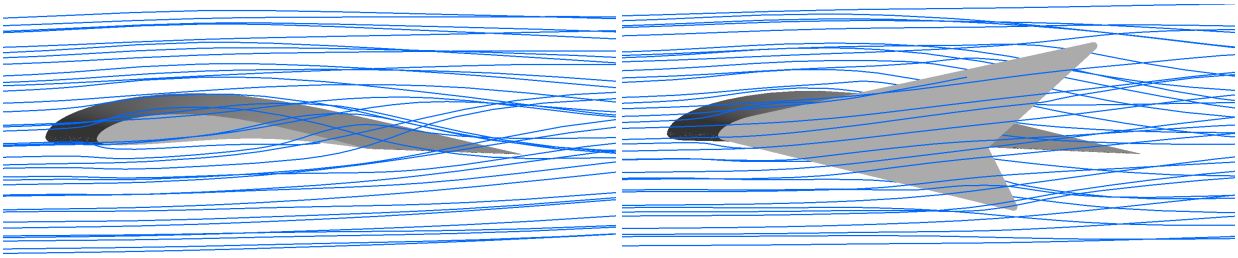

(a) Plain Wing **(b)** Winglet

Figure 4.11 – Streamline Comparison

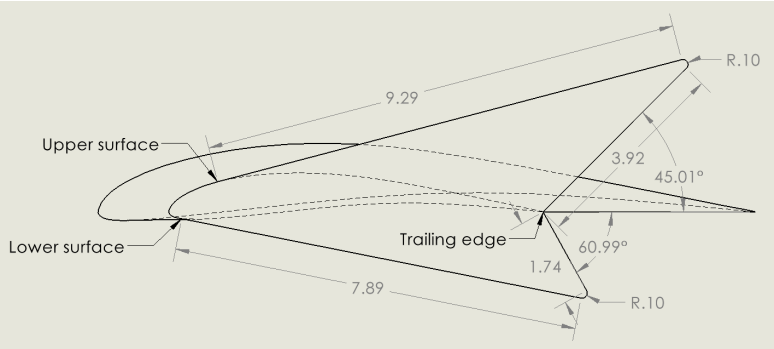

Figure 4.12 – Winglet Geometry

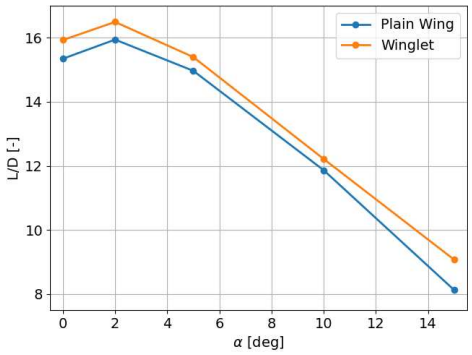

Figure 4.13 – L/D Comparison

effectively reduced the effects of this vortex. Its design was based on the vortex size near the trailing edge. An effort was made to reduce any additional drag and prevent regions of high vorticity by making the winglet tangent with the airfoil so that it was flush. Looking at Figure 4.11b shows that the winglet prevents air on the lower surface from moving onto the upper surface. Instead, the air mixes at the tips of the winglet creating two vortices that merge downstream of the wing. This can be seen in Figure 4.14 where isosurfaces of constant vorticity are shown. The vortex on the plain wing grows rapidly starting near the three-quarter chord position. In the winglet case, vorticity was primarily generated near the winglet tips and grew a small amount before merging and dissipating. It was also noted that the vortex on the plain wing appears to be longer than in the winglet case. This was to be expected as the vorticity was more concentrated and thus dissipates its energy to the surroundings faster. In the winglet case, on the other hand, the vortices dissipate their energy more slowly and were more influenced by convection. These vorticity diagrams also reveal an important effect of the winglet. Circled in red in Figure 4.14a is a region of vorticity sitting on the wing surface. For this to exist the flow must not be moving cleanly over the surface in this region. Therefore, we can further verify that the winglet improved the performance of the wing. These conclusions are supported by Figure 4.13 which shows the lift-to-drag ratio of the plain wing with the winglet. Overall, lift was increased 3.74%, drag decreased by 1.78%, and lift-to-drag ratio increased by 4.00%. In terms of mission performance, this should allow for a faster time in Mission 2 as well as more laps completed in Mission 3. Stability should not be heavily affected and will likely only see a slight decrease in trimmed angle of attack.

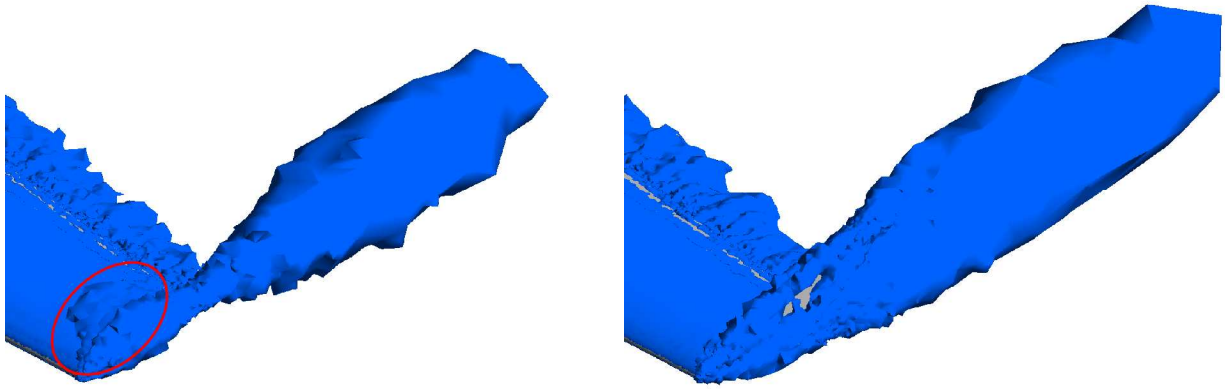

(a) Plain Wing **(b)** Winglet

Figure 4.14 – Vortex Comparison

4.5 Structures

The wing spars where designed to sustain a maximum load of 2.5 g. Stress paths followed a single main spar consisting of aircraft plywood sections joined through joints and cyanoacrylate adhesive (CA). The fuselage contains all intended sensor pod storage containers, and distributes shear stress incurred during flight. It is both lightweight and as aerodynamic as possible. Additionally, the sensor pod deployment is housed in the aft cargo bay just before the fuselage. The deployment structure and equipment are fixed features and will remain during each mission configuration.

4.6 Propulsion

Initial restrictions for the propulsion system were providing enough static thrust for takeoff and maintaining a high in flight cruise speed. After initial calculations were completed using Equation 4.13, static thrust for take off was sufficient even with Mission 2 payload. The thrust to weight ratio was sufficient for each mission configuration. The main challenge of the propulsion system was to find a battery, motor, and propeller combination that satisfied the cruise speed and flight time requirement.

$$T = \frac{1.44W^2}{\rho s C_{L,\max} g s'} \tag{4.13}$$

Where:
T = Thrust
W = Weight
ρ = Air density
s = Span
$C_{L,\max}$ = Coefficient of lift
g = Gravitational constant
s' = Takeoff distance

A LiPo battery was chosen over NiMH and NiCd due to higher energy and power density. Two 3S LiPo batteries with different discharge rates were analyzed in combination with three motors and various propellers. A discharge rate of 2200mAh was chosen because it was the lightest battery that provided enough power to provide the desired thrust and speed. MotoCalc, a propulsion analysis tool, was used to find motors that met weight, airspeed, flight time, and thrust requirements when paired with a 3S 2200mAh LiPo battery.

Table 4.6 shows the top six motor, battery, and propeller combinations along with their weights and thrust. All combinations had a flight time of over 10 minutes while maintaining a cruise speed of 41 mph. The final propulsion combination was a 3S 2200mAh Ovonic LiPo battery, E-Flite Park 480 motor, and 12x7 propeller. The chosen combination had the best thrust to weight ratio. As described in section 8.2, a thrust

Table 4.6 – Propulsion Combinations Considered

Motor	Kv	Battery/cells	Max Current Draw/A	Propeller	Static Thrust/lbs	Weight of System/lbs
E-Flight Power 25	870	3 cell (2200)	75.6	12x8	6.87	1.58
RimFire .10	1250	3 cell (2200)	40.4	10x7	2.58	1.05
E-Flite Park 480	910	3 cell (2200)	49.7	12x7	4.45	1.13
E-Flight Power 25	870	3 cell (3300)	75.6	12x8	6.87	1.99
RimFire .10	1250	3 cell (3300)	40.4	10x7	2.58	1.46
E-Flite Park 480	910	3 cell (3300)	49.7	12x7	4.45	1.54

stand was used to verify the theoretical thrust values and whether the battery could power the motor for 10 minutes.

4.7 Predicted Aircraft Performance

Each mission was simulated using the same assumptions and parameters used in the score analysis, namely using an air density taken from historical data near the Tucson flyoff site in April. The Mission 2 score assumed six containers completed in 1.5 minutes. Mission 3 assumed a maximum of 20 laps completed with a 10 in. sensor pod weighing 32 oz. The results from the simulated missions are outlined in Table 4.7 below. Lift-to-drag ratio for Mission 3 shows values for when the sensor pod is stowed and deployed. The deployed condition is in parentheses.

Table 4.7 – Preliminary Design Characteristics

Parameter	Mission 1	Mission 2	Mission 3
$C_{L,\max}$ [–]	1.40	1.40	1.40
$C_{L,\text{cruise}}$ [–]	0.67	0.73	0.62
e [–]	0.98	0.99	0.97
C_{D0} [–]	0.02	0.02	0.02
$L/D_{\max}$ [–]	16.84	18.10	17.68 (5.33)
L/D_{cruise} [–]	16.53	17.19	17.67 (2.97)
W/S [oz/in^2]	19.39	34.75	27.07
v_{cruise} [ft/s]	38.9	49.9	47.4
v_{stall} [ft/s]	29.5	39.4	34.8
Gross Weight [lbf]	5.05	9.05	7.05
Mission Score	1.00	1.46	2.26

5 Detail Design

5.1 Dimensional Parameters

The airframe dimensions did not vary between the preliminary and detailed design phases as structural analysis, propulsion tests, and aerodynamic analysis yielded ideal results. The final overall dimensional

Table 5.1 – Final Aircraft Dimensions

Fuselage		Wing	
Total Length	51 in.	Wingspan	60 in.
Nose Length	5 in.	Root Chord	12.75 in.
Empennage Length	14 in.	Tip Chord	7.25 in.
Width	3.31 in.	Mean Chord	10 in.
Height	4.20 in.	Aspect Ratio	6
Vertical Stabilizer		Planform Area	600 in.^{2}
Height	6 in.	Incidence	2 deg.
Root Chord	4.13 in.	**Horizontal Stabilizer**	
Tip Chord	2.50 in.	Span	20 in.
Mean Chord	3.38 in.	Chord	4.25 in.
Tip Offset	1.63 in.	Incidence	-1 deg.
Distance from LE	36 in.	Distance from LE	36 in.

parameters are listed below in Table 5.1. The structural components worked around volumetric constraints created by the aerodynamic design. Areas with insufficient volume were reinforced with additional material. These considerations were taken into account when designing the final competition aircraft.

5.2 Structural Components

The primary structural considerations were aerodynamic performance and manufacturing feasibility. Additionally structural weight and rigidity were always considered.

Regarding flight loads, the main concern will be aerodynamic stress and stress due to the motor. The thrust and torque generated by the motor is a considerable factor regarding the wing mounted motor design. The aerodynamic load comprises of stress due to aerodynamic forces such as lift and drag. Both of these loads will be primarily absorbed and distributed by the wing structure.

5.2.1 Wing

To minimize the structural weight of the wing, a balsa and plywood build with a tensile outer skin was utilized. Aircraft-grade plywood was used for structural hard points and balsa was used everywhere else to decrease weight. The main structural member is an I-beam spar with vertically mounted plywood for increased rigidity and horizontally mounted balsa for reduced weight. The central spar passes through a series of 1/8 in. balsa ribs that preserve the aerodynamic profile. The wingtips include a mounting point for winglets that are manufactured from 1/8 in. aircraft plywood. The motor mounts can be found 9 1/8 in. from the centerline and additional reinforcement behind the motor mount provide rigidity against thrust loads. The wing is mounted to the fuselage via hardpoint extensions built into the airfoils. It is then bolted to the fuselage. This layout can be seen in Figure 5.1. The flaps are located inboard and extend 40% of the wingspan, and the ailerons consist of the remaining 60%. A plain flap design was used for simplicity, as the benefits of more complex designs such as the Fowler flap were unnecessary. The control surfaces consist of pre-made balsa control surfaces that are modified to the proper dimensions. Also shown below in Figure 5.2 and Figure 5.3 are the shear force and bending moment relative to the wing span.

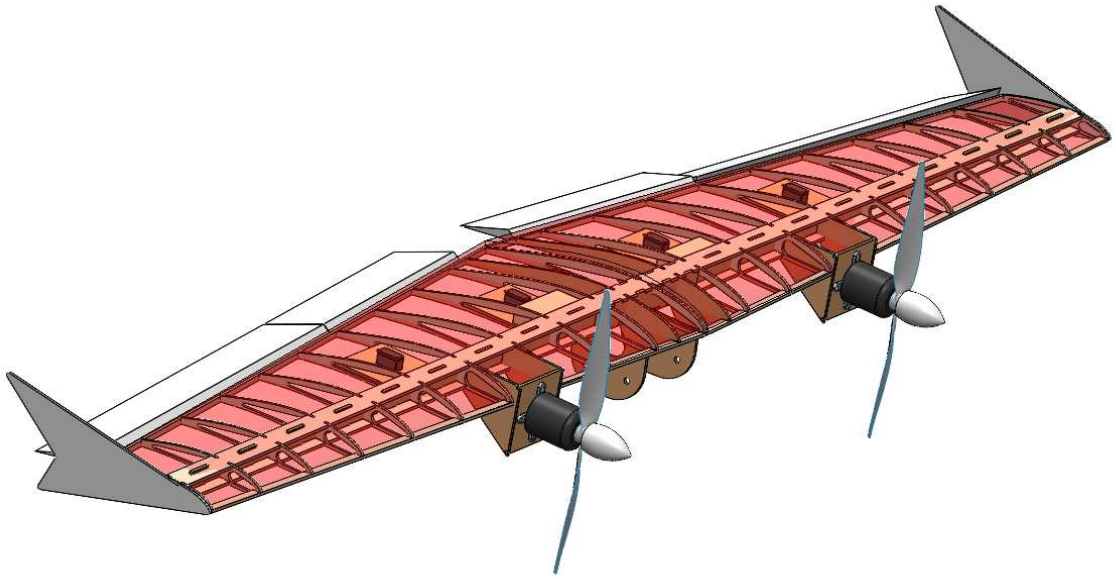

Figure 5.1 – Wing Structure

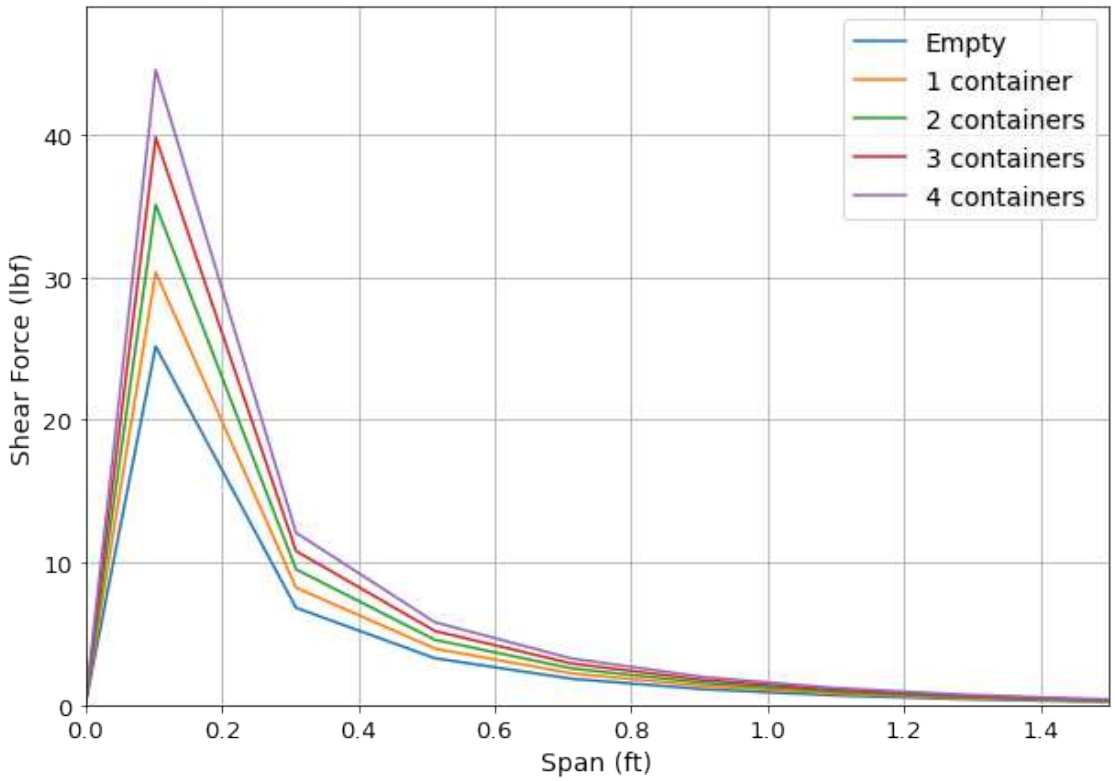

Figure 5.2 – Wing Shear Force

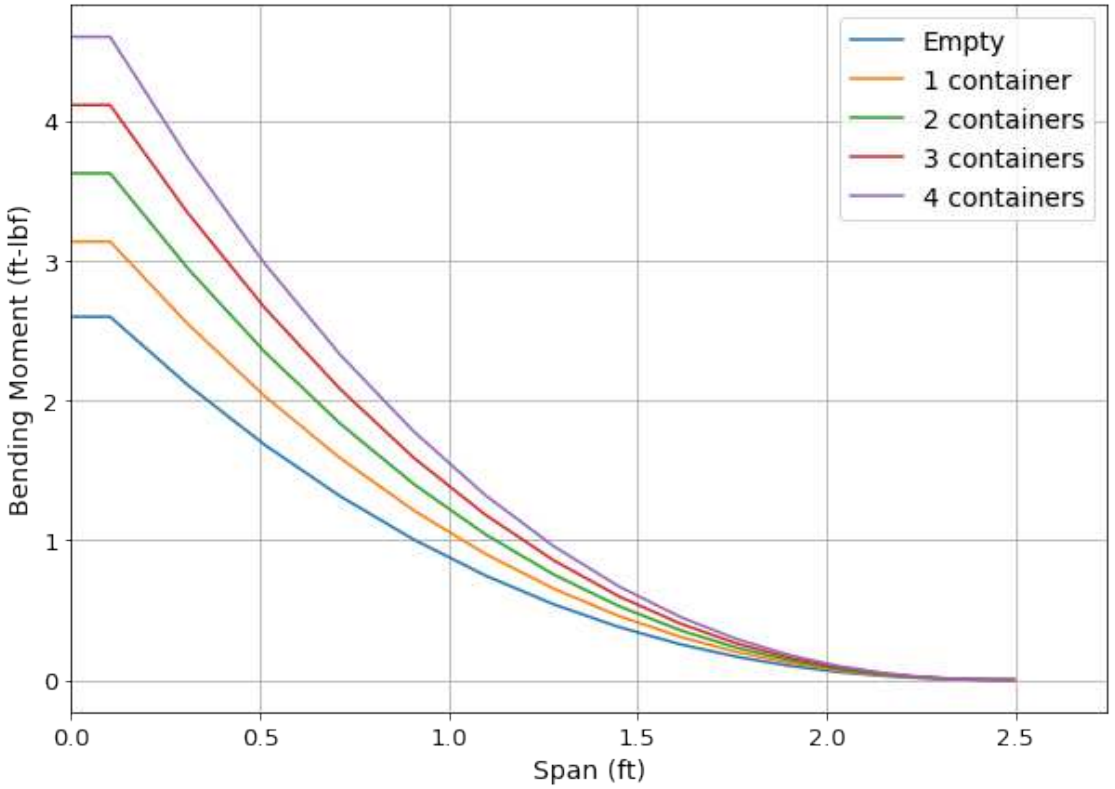

Figure 5.3 – Wing Bending Moment

5.3 Tail

The tail sections, shown in Figure 5.4 will consist of solid balsa pieces. This is possible as flat plates have been chosen for their aerodynamic properties. The structure for the horizontal and vertical stabilizers will be truss structures laser cut from 1/4 in. balsa. This allows for simplified manufacturing, while remaining rigid enough for optimal flight performance. The tail will be mounted at the end of the empennage, with the vertical stabilizer piercing the horizontal stabilizer. The assembly will be secured with bolts through protruding extrusions that pierce through the bottom of the empennage. The elevator and rudder consist of solid balsa pre-made control surfaces that are modified to the proper dimensions. The structure will be covered in Monokote, to both preserve the aerodynamic profile and increase rigidity of the tail. The servos to control the elevator and rudder will be mounted on the empennage and control linkages will connect them.

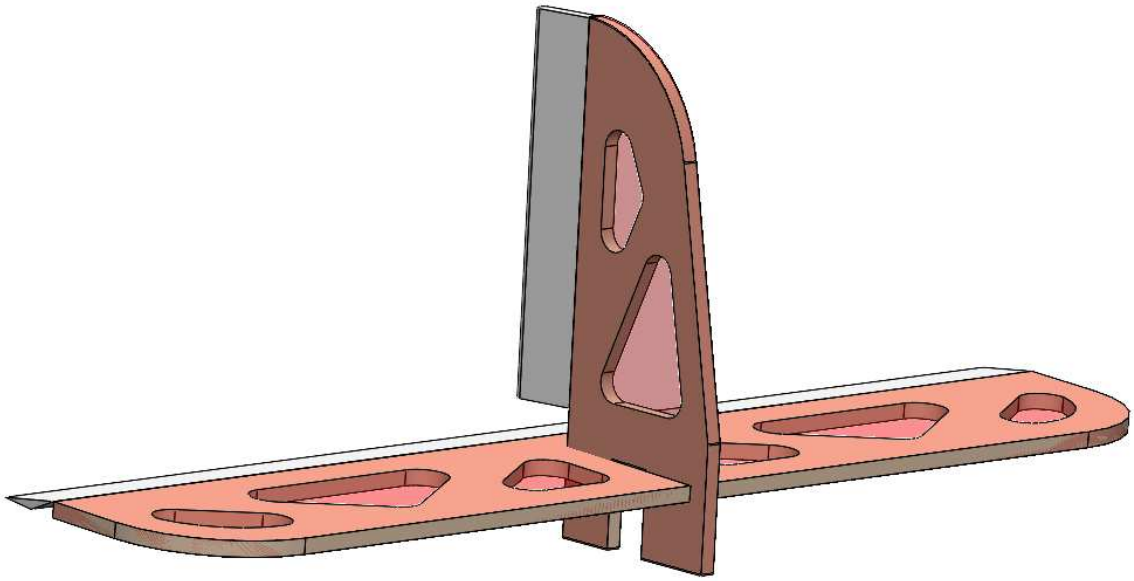

Figure 5.4 – Tail

5.3.1 Fuselage

The fuselage design was chosen based on previous manufacturing experience. A semi-monocoque design was initially considered but complexities in manufacturing resulted in a truss structure being used. The nose cone retained a semi-monocoque structure to reduce parasitic drag. The nose cone is mobile, rotating about a hinge and is secured during flight via canopy locks. The design shown in Figure 5.5 enables access to the avionics and payload storage. The extended nose section allows additional room for component placement and weight balancing. The fuselage and nose cone are constructed with 1/8 in. aircraft plywood for optimal rigidity and flight characteristics. The interior can be accessed via the nose cone hatch in the front or the aft sensor pod deployment hatch. The entire structure is covered with Monokote to preserve the aerodynamic profile.

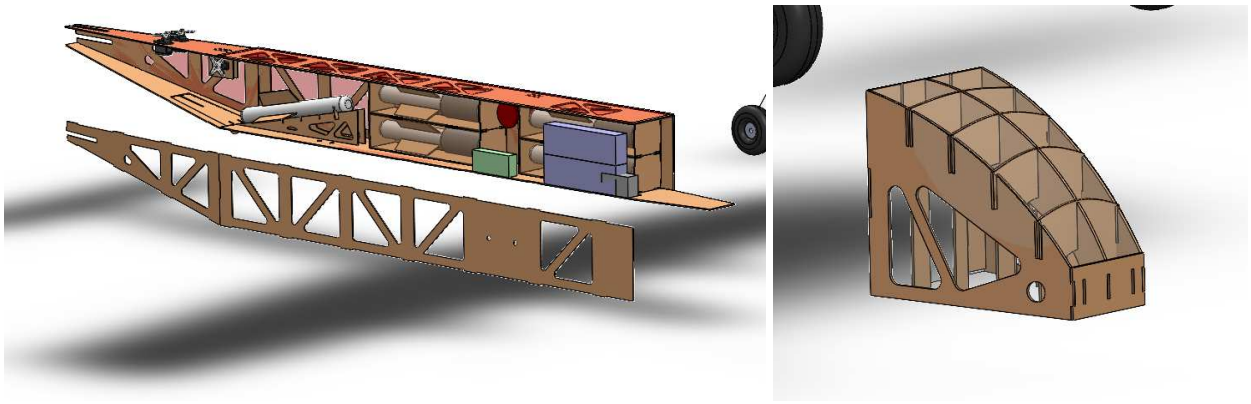

(a) Fuselage Truss Structure **(b)** Nose Cone Design

Figure 5.5 – Fuselage Components

5.3.2 Empennage

The empennage consists of a plywood panel truss similar to the fuselage for a rigid and lightweight design. This was also chosen to retain a similar manufacturing process for all components for simplicity. The tapered design allows for decreased weight and drag, as well as increased maximum tip-back angle for take-off. This can also be seen in Figure 5.5.

5.4 Systems and Sub-Systems

5.4.1 Sensor Pod

The sensor pod was designed to be 1 lbf. each, and the airframe allows storage up to 4 sensors. The sensor pod is 8 in. long and has a constant diameter of 1 in., shown in Figure 5.6. The sensor pod will be manufactured from polystyrene foam board. This material was chosen due to its simplified manufacturing process, allowing an aerodynamic profile while investing minimal manufacturing time. Additionally, polystyrene is readily available and wood was reserved for airframe structural components.

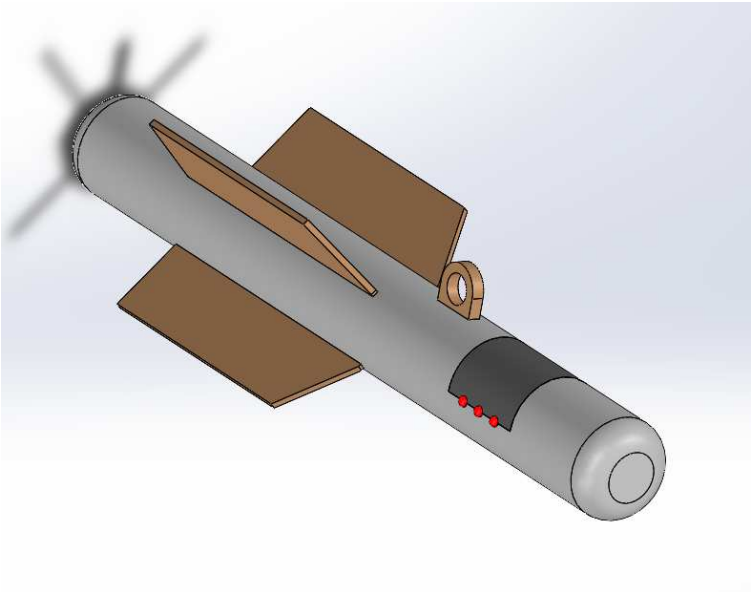

Figure 5.6 – Sensor Pod

The sensor pod circuit is a sequential circuit and is assembled and soldered onto a circuit board, utilizing integrated circuits. The breadboard shown in Figure 5.7 reflects the circuit proposed in Section 4.3. The pod will be powered by an onboard 3v battery, and signals will be provided by the aircraft receiver. The entire assembly will be accessed through a cut-out hatch. The pod has 6 slots cut out to accommodate for the LED's. The 6 LED's, 3 on each side, will be lit sequentially given an input signal shown previously. The switch represents the transmitter input signal. Three 74HC00 Quad NAND gates and two 74HC74 D-Flip-Flops were used to provide the logic for the circuit.

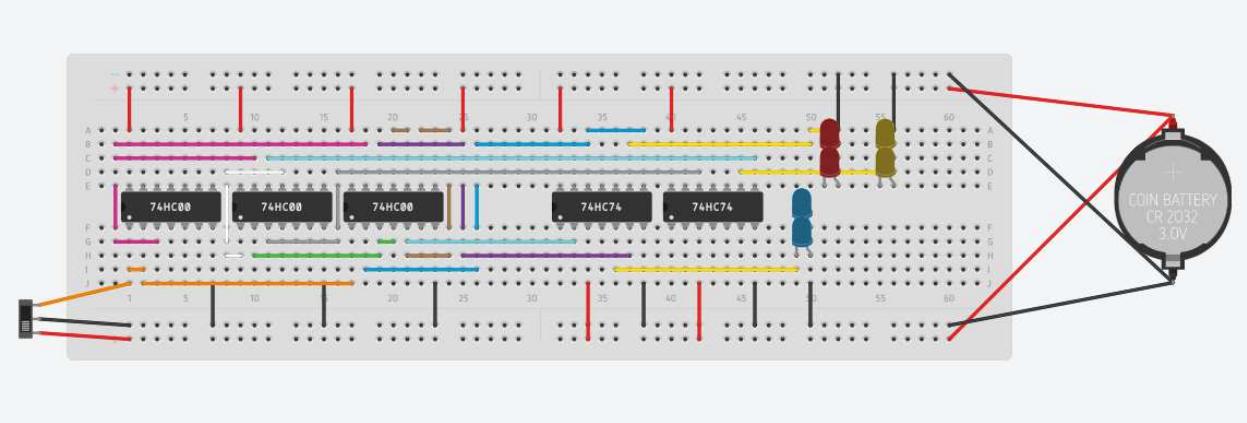

Figure 5.7 – Sensor Pod Circuit Assembly

5.4.2 Shipping Container

The shipping container, seen in Figure 5.8, was engineered to fit the sensor pod and its required length of tow cable. A box structure was selected for simplicity made of 1/16 in. sheets of plywood. The container was designed to protect the sensor, and is insulated with electronic packing foam to protect stored components.

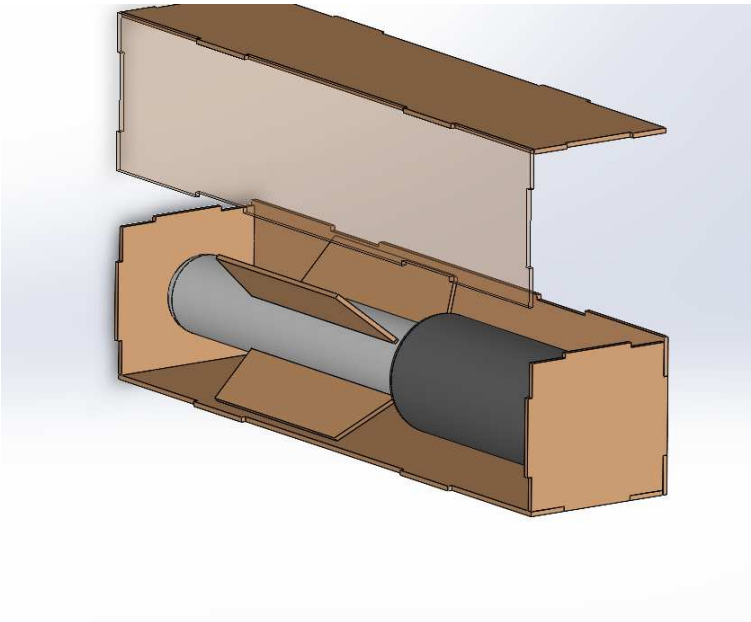

Figure 5.8 – Sensor Pod Storage Container

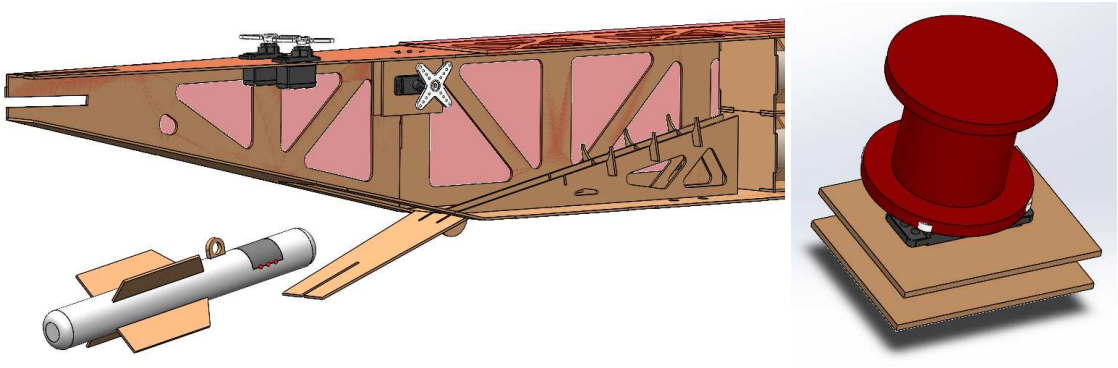

(a) Deployment Ramp & Door **(b)** Deployment Spool

Figure 5.9 – Deployment System

5.4.3 Sensor Pod Deployment

The sensor pod deployment mechanism, shown in Figure 5.9 is a gravity operated, ramp system placed in the aft cargo section of the aircraft. The sensor pod itself rests upon a ramp and is held in place via tension from the deployment spool. The ramp itself contains a holding structure and the spool tension provides retention. This deployment spool is driven by a servo operated by a knob on the transmitter. This spool is placed in the wing mounting section to minimize the impact of tension during flight. Additionally there is a door on the empennage floor which allows the pod to exit. Once tension has been released, the weight of the pod will accelerate it outside the aircraft. For retraction, the spool will wind itself up and the sensor pod will be guided back onto the deployment ramp.

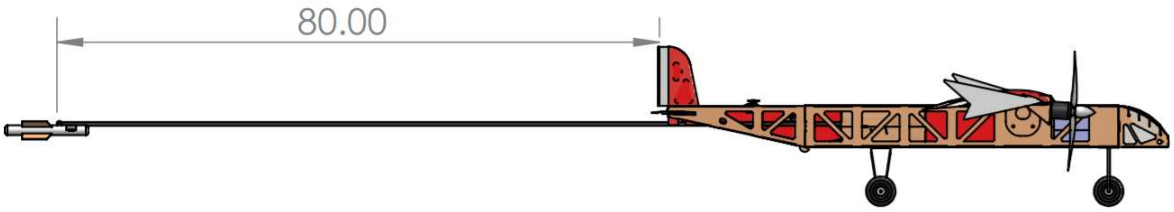

Figure 5.10 – Sensor Pod In-Flight

5.4.4 Propulsion System

The aircraft's dual motors will be mounted on hardpoints 9 1/8 in. away from the centerline of the aircraft. These hardpoints will be manufactured from 1/8 in. aircraft plywood for rigidity. Static motor testing confirmed that the capacity and thrust requirements would be met with the following propulsion package shown below in Table 5.2.

Table 5.2 – Propulsion System Components

Criteria	Weight
Motor	2x E-flite Park 480 910Kv
Battery	2x 2200 3S 2200 mAh LiPo
ESC	Spektrum AR8010T

5.4.5 Landing Gear

A tricycle configuration is used for the landing gear. It consists of nose mounted and wing mounted wheels, encompassing the CG. This configuration was chosen to accommodate the sensor pod deployment system. It was designed to prevent contact with the sensor pod and tow cable while in flight. It is tall enough to accommodate the maximum proposed propeller size. With no P-factor or torque effects on takeoff/landing, the landing gear contains no steering ability for simplicity and weight minimization. Both the nose and main gear can be seen below in Figure 5.11.

Figure 5.11 – Landing Gear

Table 5.3 – Landing Gear Function Matrix

Criteria	Weight	Fixed	Retractable
Drag	30	1	2
Weight	25	2	1
Complexity	25	2	1
Manufacturing	20	2	1
Total	100	175	125

5.5 Weight and Balance

Component placement for each mission is shown in Table 5.4. All distances are measured from the leading edge of the aircraft using the Aircraft-Based Back-Starboard-Up coordinate system. In this system x points from the nose to tail, y points from the fuselage centerline to starboard or the right wingtip, and z completes the right-hand coordinate system by pointing up. For each mission, stability is ensured by using the propulsion batteries as a ballast to achieve the desired CG location. The deployed sensor pod row uses the effective weight caused by the tension in the cable applied at the spool.

Table 5.4 – Weight Balance For Each Mission

Component	Weight [lbf]	x [in.]	y [in.]	z [in.]
General				
Fuselage	1.25	2.000	0.000	-1.500
Wing	1.25	4.435	0.000	0.329
Motors	0.80	0.000	±10.500	0.000
H-Stabilizer	0.100	37.791	0.000	-0.031
V-Stabilizer	0.100	38.134	0.000	2.519
Mission 1				
Batteries	0.750	0.000	1.000	-2.500
Mission 2				
Batteries	0.750	0.000	1.000	-2.500
Containers	4.000	4.000	1.250	-1.500
Mission 3				
Batteries	0.750	-5.000	1.000	-2.500
Sensor Pod Stowed	1.000	16.200	0.000	-2.000
Sensor Pod Deployed	2.000	3.500	0.000	-0.250

5.6 Flight Performance

Expected performance is shown in Table 5.5. These results come from the XFLR5 analysis of the final design as well as equations derived from basic aircraft flight mechanics equations. L/D for mission 3 has an additional value in parentheses. The value outside the parentheses is for the stowed condition and the value in the parentheses is for the deployed condition. Below, Table 5.6 shows the assumptions made for score analysis and the expected results for each mission.

Table 5.5 – Predicted Aircraft Performance

Parameter	Mission 1	Mission 2	Mission 3
$C_{L,\max}$ [–]	1.40	1.40	1.40
$C_{L,\text{cruise}}$ [–]	0.67	0.73	0.62
e [–]	0.98	0.99	0.97
C_{D0} [–]	0.02	0.02	0.02
$L/D_{\max}$ [–]	16.84	18.10	17.68 (5.33)
L/D_{cruise} [–]	16.53	17.19	17.67 (2.97)
W/S [oz./in.^{2}]	19.39	34.75	27.07
v_{cruise} [ft/s]	38.9	49.9	47.4
v_{stall} [ft/s]	29.5	39.4	34.8
v_{takeoff} [ft/s]	30.8	41.2	36.3
Takeoff Distance [ft.]	44.0	90.5	65.5
Gross Weight [lbf.]	5.05	9.05	7.05

Table 5.6 – Mission Scoring Predictions

Parameter	Mission 1	Mission 2	Mission 3
Completion	1.0	1.0	2.0
$(N_{\text{con}})_{\text{IIT}}$	–	4	–
$(T_{M2})_{\text{IIT}}$ [min.]	–	2.18	–
$(N_{\text{con}}/T_{M2})_{\max}$ [1/min]	–	4.00	–
$(N_{\text{laps}})_{\text{IIT}}$	–	–	13
L_s [in.]	–	–	8
W_s [oz.]	–	–	16
$(N_{\text{laps}} \times L_s \times W_s)_{\max}$ [in·oz]	–	–	6,400
Mission Score	1.0	1.46	2.26
Total Mission Score		4.72	

5.7 Drawing Package

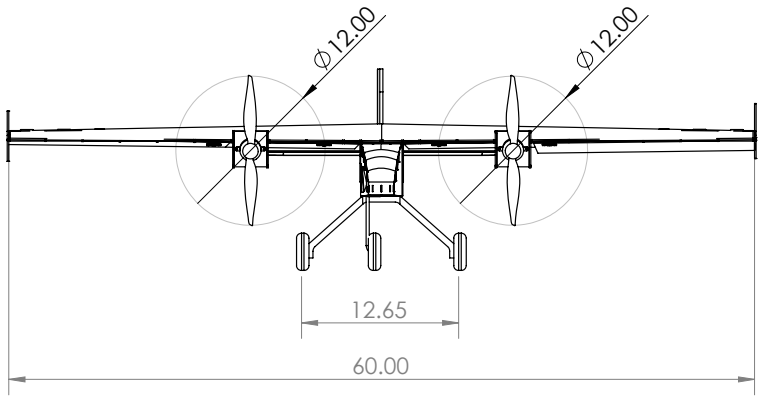

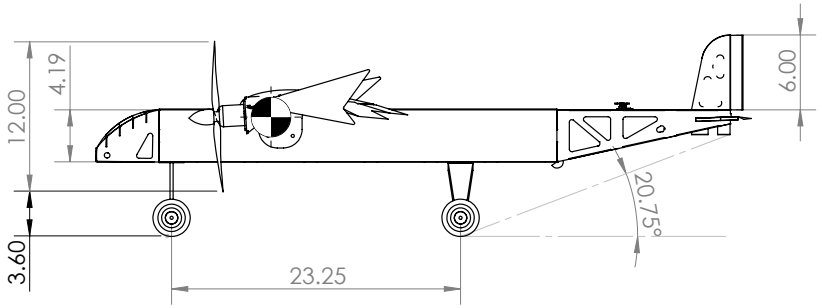

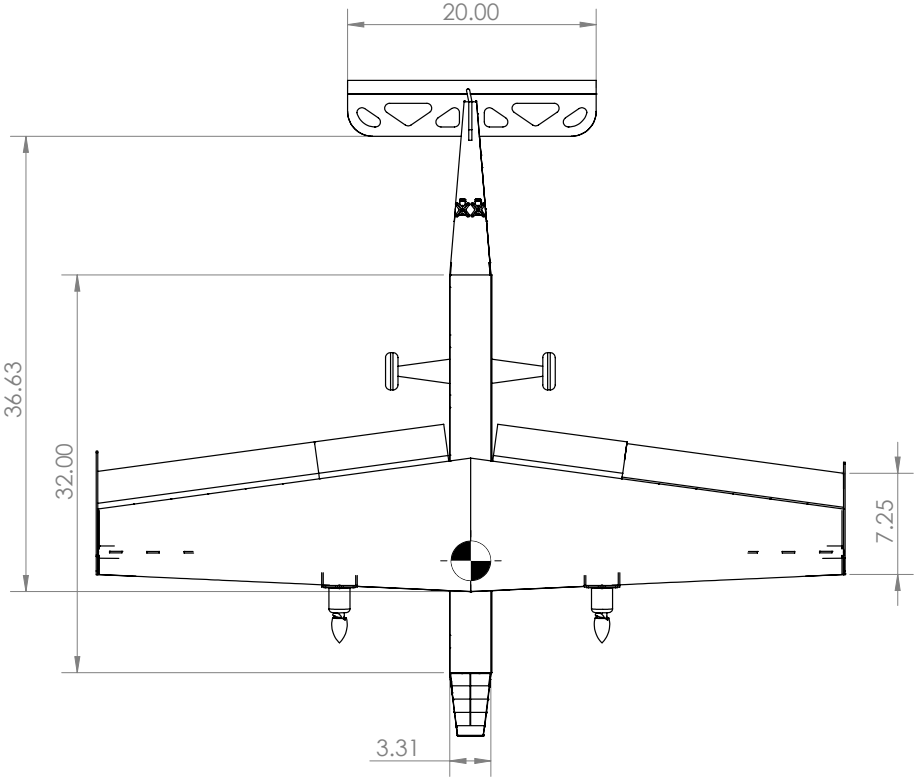

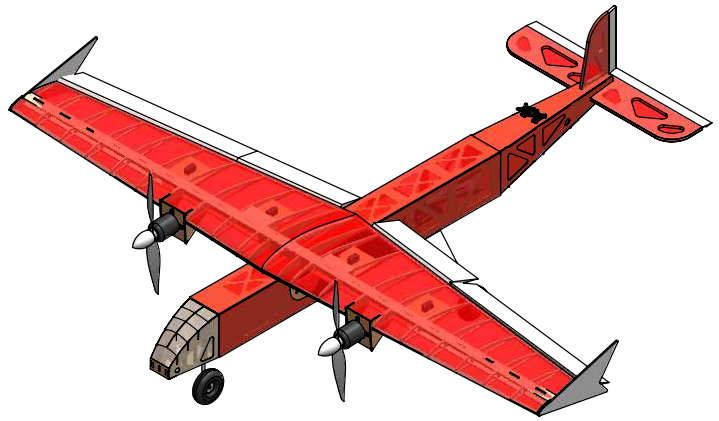

Illinois Institute of Technology AIAA Design/Build/Fly 2021	
TITLE: BearHawk	
UNLESS OTHERWISE SPECIFIED: DIMENSIONS ARE IN INCHES	
DRAWN BY: Christian Comillas	SIZE B DWG. NO. Aircraft-3-View
	SCALE: 1:10 Drawing Package SHEET 1 OF 3

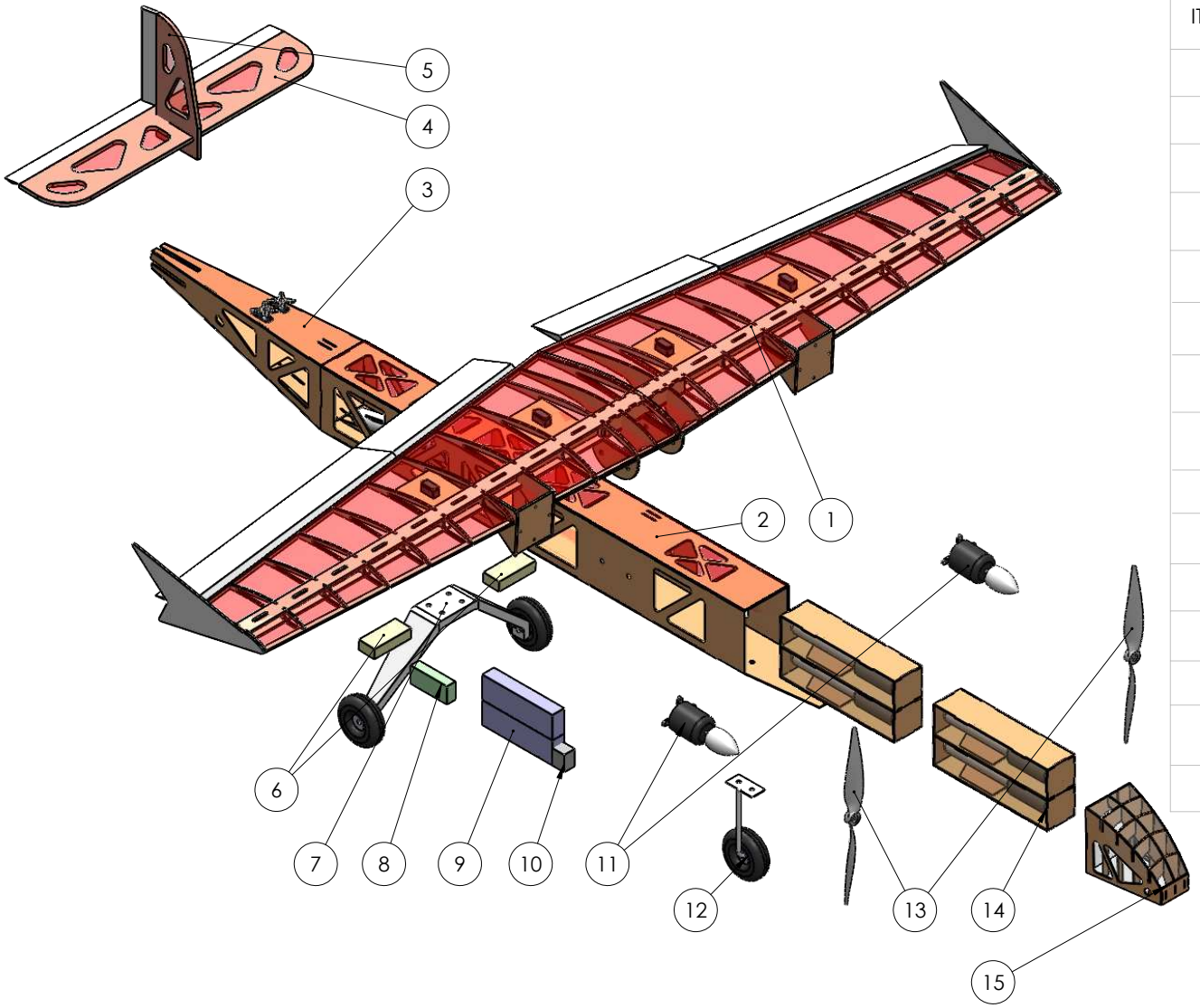

ITEM NO.	COMPONENT	DESCRIPTION	QTY
1	Wing	Aircraft Plywood, Balsa, Monokote	1
2	Fuselage	Aircraft Plywood, Monokote	1
3	Empennage	Aircraft Plywood, Monokote	1
4	Vertical Stabilizer	Balsa, Monokote	1
5	Horizontal Stabilizer	Balsa, Monokote	1
6	ESC	Caslte Creations Phoenix HV 60	2
7	Landing Gear	Aluminum	1
8	Reciever Battery	1S LiPo Battery	1
9	Motor Battery	2200 mAh Ovonic 3S	2
10	Reciever	Spektrum AR8010T	1
11	Motor	Park 480	2
12	Nose Gear	Aluminum	1
13	Propeller	12" x 7"	2
14	Sensor Pod Container	Aircraft Plywood	4
15	Nose Cone	Aircraft Plywood, Monokote	1

Illinois Institute of Technology
AIAA Design/Build/Fly 2021

TITLE:
BearHawk

UNLESS OTHERWISE SPECIFIED:
DIMENSIONS ARE IN INCHES

DRAWN BY:
Christian Comillas

SIZE B | DWG. NO. Aircraft Overview

SCALE: 1:6 | Drawing Package | SHEET 2 OF 3

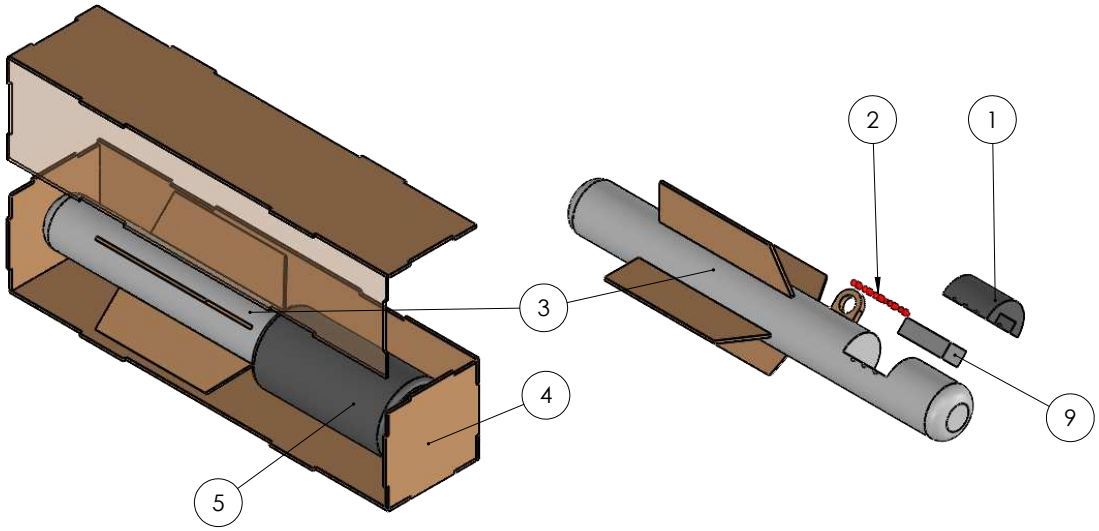

ITEM NO.	COMPONENT	DESCRIPTION	QTY
1	Pod Cover	Polystyrene	1
2	LED	SPECS	6
3	Sensor Pod	Polystyrene, Plywood Fins	1
4	Storage Container	Aircraft Plywood, Insulating Foam	4
5	Tow-Cable	100 in. Para-chord	1
6	Deployment Ramp	Plywood Structure	2
7	Deployment Servo	Hi-65MG	1
8	Spool	3D Printed ABS	1
9	Sensor Circuit	Circuit Board	1

Sensor Pod Containers will be representative weights for M2 but are shown to contain necessary equipment.

Sensor Pod will not be present on deployment ramp for M3

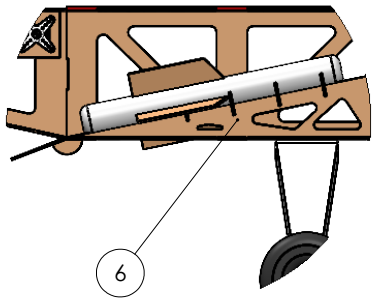

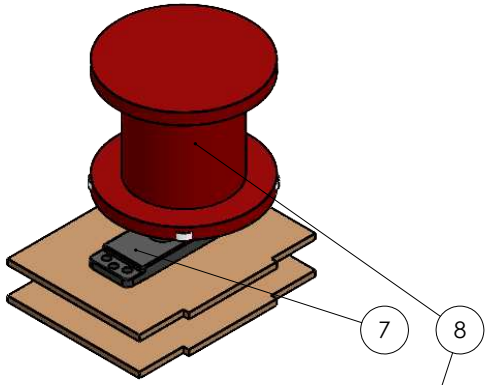

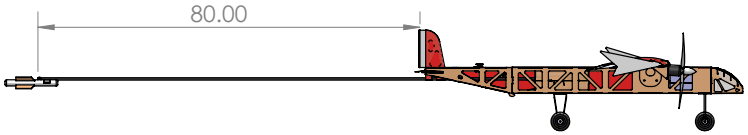

DETAIL A
SCALE 1 : 4

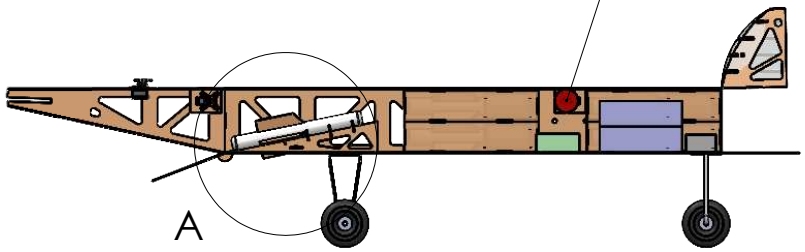

A

Illinois Institute of Technology
AIAA Design/Build/Fly 2021

TITLE:
BearHawk

UNLESS OTHERWISE SPECIFIED:
DIMENSIONS ARE IN INCHES

DRAWN BY:
Christian Comillas

SIZE B | DWG. NO. Subsystem View

SCALE: 1:8 | Drawing Package | SHEET 3 OF 3

6 Manufacturing Plan

A number of manufacturing processes were investigated to determine the best option for the aircraft. Each component was built with the most suitable material as determined by the following processes.

6.1 Manufacturing Processes Investigated

6.1.1 Foam

The benefits of using foam for lifting bodies includes high rigidity, strength, and easier assembly. However, foam is considerably heavier than balsa and needs specific tools, such as a computer numerical controlled (CNC) wire-cutter. Manufacturing a fuselage out of foam is not practical, as it breaks easily without sufficient thickness. This would result in thick fuselage walls or additional structural members. As a result, foam structures are far heavier and less reliable for an aircraft of this size.

6.1.2 Balsa

The benefits of using balsa for the lifting bodies includes being light weight, ease of manufacturing, and having a high strength to weight ratio. While balsa construction is more time consuming than foam, balsa assembly is still fast due to its simplicity. This is due to the usage of laser cutters, which easily create designed parts from raw material. Balsa was chosen for wing components due to ease of manufacturing, light weight, and high unidirectional strength. The team's access to CAD allows precise design with both balsa and plywood. The main drawback with wood based designs are the geometric constraints regarding aerodynamic profile.

6.1.3 Plywood

The benefits of using plywood is its rigidity in all directions, but it weighs more than balsa. As a result plywood was used for more structurally demanding components such as the fuselage and outboard wing spar. The weight increase was insignificant compared to the benefit of rigidity. Thin plywood has similar weight as thick balsa but also has a higher elastic modulus. Both plywood and balsa construction require parts to be designed and laser cut in order to have the highest precision. This necessitates some knowledge in the area, but has a much shallower learning curve than other methods.

6.1.4 Composites

Composites provide the highest strength-to-weight ratio, and are able to undergo high deflection before failure. Complex shapes become available when using composites, expanding airframe geometry possibilities. The team was interested in exploring integrating composite manufacturing into the project, however complications regarding COVID-19 limited opportunities to train members. With minimal prior experience, the team elected to forgo composite manufacturing. Additionally acquiring composites has proven expensive and difficult this season, further discouraging exploring its implementation.

6.1.5 3D Printing

3D printing allows the production of complex shapes and components. However, even at minimal fill settings this method creates heavy components, relative to the other methods. The team has access to multiple 3D printers that vary in precision and material selection. Overall, this process was utilized sparingly for specific components such as the sensor pod tow cables spool.

6.2 Manufacturing Process Selection

Manufacturing techniques were chosen using a selection matrix to determine where each technique excels. From this, each component could be assigned a technique. The significance of each parameter is described below.

Weight: Materials with a lower weight are highly beneficial to the design. A low weight would allow for more payload to be carried, resulting in a higher score.

Strength: Having enough strength for the particular application will ensure the aircraft remains intact during all phases of flight–especially in off-design conditions.

Ease of Manufacture: The ability to easily manufacture the components of the aircraft allows for faster build times, leading to the ability to test more flight iterations. It is especially important as in-person manufacturing time is limited and difficult to organize due to COVID-19 regulations during the 2020-2021 season.

Team Experience: Previous experience with the chosen manufacturing techniques will ensure that less setbacks are encountered during the construction process. This was important for the 2020-2021 season as limited physical meetings reduces exposure to new manufacturing techniques.

Table 6.1 – Manufacturing Technique Selection Matrix

Criteria	Weight	Foam	Balsa	Plywood	Composites	3D-Printing
Ease of Manufacture	35	5	4	3	1	2
Weight	25	2	4	3	5	1
Strength	25	1	2	4	5	3
Team Experience	15	3	5	4	1	2
Total	100	295	365	340	300	200

Using the results from Table 6.1, a combination of balsa and plywood was chosen. The following section outlines the materials chosen for each portion of the aircraft. Due to the majority of the aircraft utilizing wood construction, laser cutting was used on all parts to ensure accuracy. The wood construction requires a sheeting over the airframe to maintain its aerodynamic profile. This was done using an adhesive, heat-shrink mylar skin called Monokote.

6.3 Component Manufacturing

6.3.1 Wing Structure

The main wing structure consists of a balsa-plywood build up. This was done to utilize each material's strengths appropriately. The various members were designed with tongue and groove joints. This allowed the laser-cut wood pieces to be jigged and aligned. The laser-cut pieces were then attached using CA glue. before the whole wing was covered in Monokote, the leading edge was sheeted in 1/32 in. balsa wood to reinforce the aerodynamic profile. The electronics were then installed via removable panels within the wing. An example of the manufactured structural components can be seen in Figure 6.1. The control surfaces were manufactured using pre-made balsa wedges or balsa sheets and trimmed into the appropriate dimension. They were attached to the wing using point hinges.

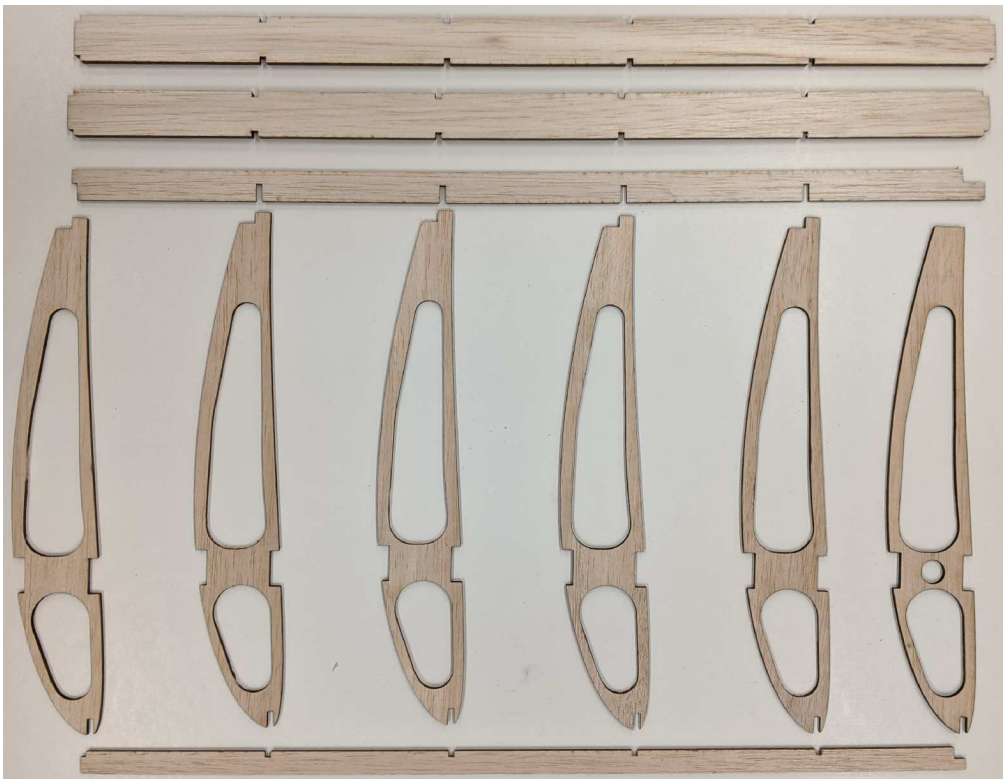

Figure 6.1 – Wing Ribs and Spar Sections

6.3.2 Tail Structure

The tail structure was manufactured utilizing a laser-cutter and 1/4 in. balsa wood. This was done to simplify design and manufacturing. The vertical stabilizer was slotted into the horizontal stabilizer. The whole assembly slots into the empennage and is bolted in place.

6.3.3 Fuselage Structure

The fuselage was constructed utilizing a plywood build up with laser-cut components. The high modulus of elasticity allowed a lightweight yet rigid fuselage design. The components contained tongue and groove joints allowing straightforward alignment and attachment. The components were attached using CA glue. Pins were used to hold the individual pieces in place while gluing, and a square was used for alignment.

6.3.4 Sensor Pod

The sensor pod was manufactured using a CNC on polystyrene foam board to focus limited manufacturing time to more flight critical components. A hatch was to be cut out by hand and sanded within ideal tolerances to accommodate for the onboard sensor circuit package, shown in Figure 5.7. The sensor pod fins where manufactured using 1/8 in. aircraft plywood for rigidity and assembled using epoxy.

6.3.5 Sensor Pod Deployment System

The built-in sensor pod deployment system consists of laser-cut 1/8 in. aircraft plywood sheets, similar to the fuselage itself. The servo system was held in place using more plywood and the spool itself was 3D printed, and adapted to directly mount onto an existing servo control arm.

6.4 Manufacturing Milestones

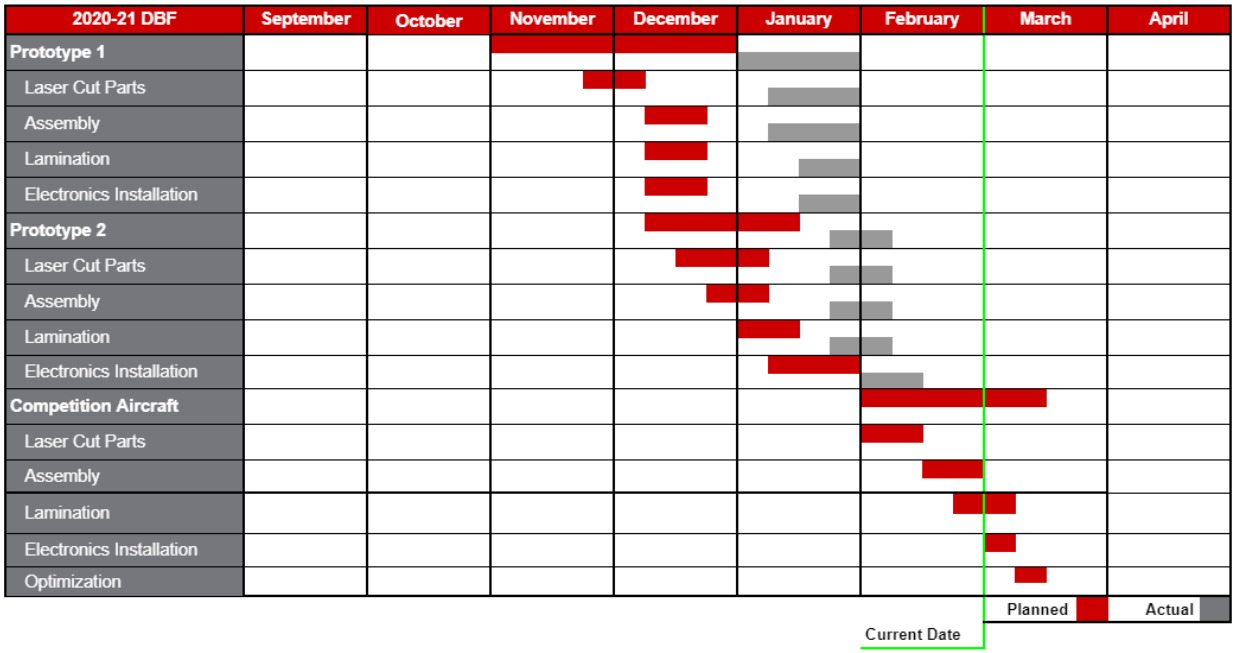

Figure 6.2 – Manufacturing Milestones

The manufacturing milestone chart, shown above in Figure 6.2, was prepared at the beginning of the season to organize the team and align sub-team manufacturing goals. This schedule was largely tentative as coordinating in-person manufacturing sessions proved difficult regarding COVID-19 regulations. As a result, a majority of the planned deadline could not be met, however, the team compensated by performing analysis remotely. Design iterations were evaluated at regular intervals and refined similar to the physical manufacturing cycle. Potential issues were highlighted and taken into consideration to prepare for the next design interval.

7 Testing Plan

Theoretical predictions of aircraft performance were tested to assess their validity. In addition, tests were performed to find the ideal combination of the subsystems: aerodynamics, propulsion, and structures. Subsystem relationships were tested for each mission to determine maximum efficiency of overall aircraft performance.

7.1 Testing Schedule

There are three main categories that are to be tested: aerodynamics, propulsion, and structures. The testing schedule and objects are broken down in Figure 7.1 below:

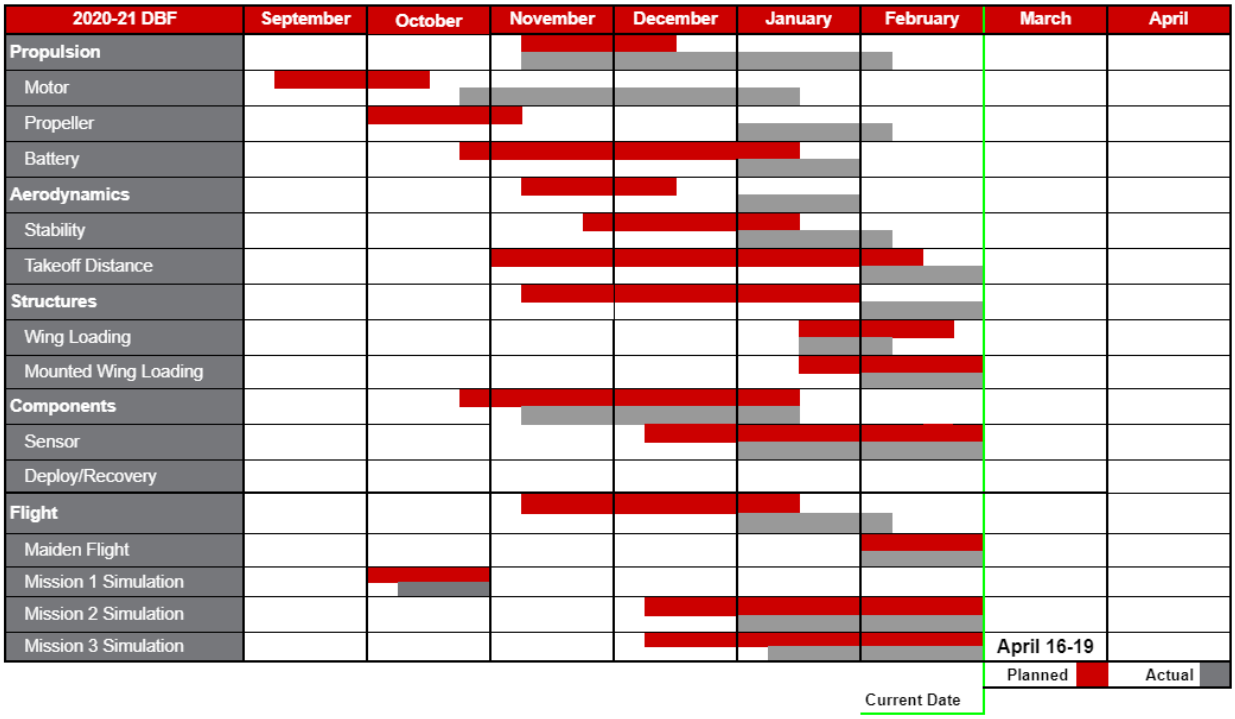

Figure 7.1 – Testing Milestone Chart

7.2 Test Objectives

The goals desired in testing are to ensure satisfactory execution of various subsystem constructions that meet their associated design parameters. In addition, the sensor pod deployment and recovery mechanism will be tested to ensure appropriate function.

7.2.1 Aerodynamics

The main goal of the aerodynamic testing will be to observe takeoff performance, as well as stability and controls. Stability and controls will be evaluated by experienced pilot feedback in comparison to the simulations conducted via CFD.

7.2.2 Propulsion

The objective of the propulsion testing is to verify the motor, battery, and propeller combination meet the desired high cruise speed. The endurance of the final combination will be found by analyzing voltage drop over time at both full power and cruise power. After each test, the final voltage of the battery will be

compared to the beginning value to find the voltage drain. Current draw will be analyzed by the on-board ESC and will be taken into account for future iterations. Additionally, propeller changes will be tested and analyzed to find the optimal balance of thrust and flight time.

7.2.3 Structures

The objective of structure testing is to assess the structural integrity of the design, specifically the wing through applying hydrostatic stress on the structure. The test conducted is visualized in Figure 7.2. The wing will be held at the tips and a bucket will be hung in the middle of the wing. Water will be slowly poured into the bucket, increasing the applied force until failure. In addition, a hand wingtip test is done before every flight test to verify center of gravity and wing rigidity. The wing will be lifted at the tip by two members of the team. If the wing doesn't fail or bend beyond tolerance, it will be accepted.

Figure 7.2 – Wing Loading Test

7.2.4 Performance

The objective of performance testing is to validate performance predictions provided by calculations made by the team for takeoff field length, cruise speed, lap times, endurance, and handling characteristics of the deployed sensor pod.

7.2.5 Flight Plan

The objective of the flight plan is to layout and contextualize the handling and performance of the prototype model. The flight plan is outlined on Table 7.1. Payload, objectives, and criteria of each flight is included in the plan. The criteria shows the aim of the test flight: to identify any errors or unforeseen challenges with the prototype airplane.

Table 7.1 – Flight Plan

Flight #	Payloads	Objectives	Criteria
1	Nothing	Takeoff and Landing Test	Determine stability of empty plane
2	Nothing	Mission 1 Simulation	Record # of labs within time limit
3	Sensor Pod (Stored)	Mission 2 Simulation	Stability with sensor pod stored
4	Sensor Pod (Deployable)	Mission 3 Simulation	Stability of deployed sensor

7.3 Test Flights

Flight testing is the final milestone for each prototyping phase. Through flight testing, the team will evaluate aircraft performance relative to previous iterations and theoretical performance. Flight testing effectively combines each ground subsystem test into a singular trial. Stability and controls will be adjusted using experienced pilot feedback. Structures testing was simulated through high loading aerobatic manoeuvres. Propulsion testing will be assessed through full throttle takeoff tests, speed trials, and endurance trials.

A balanced approached to flight testing was planned. The first flights will be taken cautiously and objectives will be slowly increased to push the limits of the prototype. A flight test will begin with a shakedown run, a simple takeoff and landing. It will then progress to the objectives for the run, which comprise of mission objectives. For Mission 2, the deploying and recovery mechanism will be operated. Throughout the testing day, performance will be adjusted in propulsion, configuration and control surface trim.

Upon the approach of aircraft performance limit, the team will push the known performance envelope of the design. The prototype will be expendable and observing the limits of the design will be highly desired. This will involve exceeding known safety parameters through overloading payload and decreasing lap time. Upon this stage of testing, the next iteration will be in production and loss of the active prototype will not hinder the team's progress. This aggressive performance will allow the team to pursue beneficial design changes that would otherwise remain unknown. Performance following assumptions made from the previous prototyping stage will be used to improve future iterations.

At the time of this report, the current prototype is in the process of being manufactured due to complications regarding COVID-19 regulations and material acquisition.

The team's prototype objectives can be seen in Table 7.2. Each flight test had specific design objectives to validate the effectiveness of the aircraft and its subsystems. Flight objects that are not achieved will be investigated and repeated at the team's discretion.

Table 7.2 – Flight Test Order

Flight Test Order	Aircraft	Objective
1	Prototype 1	Takeoff Landing Test
2	Prototype 1	Mission 1 Simulation
3	Prototype 2	Mission 2 and 3 Simulation
4	Prototype 3	Propulsion Testing

7.4 Flight Checklist

The team followed a pre-flight and flight checklist shown in Table 7.3, and Table 7.4. This was done to ensure proper data collection and efficiency. Each category allowed for the specific tasks regarding aircraft inspection and maintenance.

Table 7.3 – Preflight checklist

Component	Task
Fuselage (Internal)	☐ Secure and Connect the Fully Charged Battery
	☐ Receiver has All Connections Plugged in and Secured
	☐ Verify CG
	☐ Load Sensor, Shipping Container (if applicable)
Fuselage (Internal)	☐ Close and Fasten External Mechanisms
	☐ Arm Sensor Deployment/Recovery Mechanism (if applicable)
Pilot Checks	☐ Check all control surfaces with receiver
	☐ Motor Run Up
	☐ Go/No-Go

Table 7.4 – Flight checklist

Component	Task
Before Flight	☐ Propeller Secure
	☐ Fasteners Secured
	☐ Connections Secured
	☐ Battery Charged/Secured
	☐ Free/Connect Control Surfaces
	☐ Plug in Receiver Pack
	☐ Reciever Pack Connected
	☐ Shipping Container/ Sensor Connected and Secured
During Flight	☐ Sensor Pod Fully Deployed
	☐ Sensor Pod Light Visible
	☐ Sensor Pod Fully Recovered
After Test	☐ Throttle Idle
	☐ Battery Disconnected

8 Performance Results

Due to COVID-19, there were delays with manufacturing and material acquisition. This pushed back the original goal of having a working prototype before the report deadline.

8.1 Aerodynamics

A flight test will still be conducted after the report submission to evaluate the handling characteristics and gather performance data in a realistic environment. This data will be used to determine possible score for each mission, and to identify any unforeseen structural issues. Flight tests will also determine the effect of

the deployed sensor pod on the flight characteristics of the aircraft.

8.2 Propulsion

A test stand was used to verify if the chosen battery, motor, and propeller combination could produce thrust needed for takeoff and that the battery could power the motor for a minimum of 10 minutes. at cruise throttle. The thrust calculated using MotoCalc was 4.45 lbs for two E-Flite Park 480 motors. The total measured thrust was 3.2 lbs. Even though the thrust measured was lower than the theoretical value, it is still more than sufficient for takeoff for all missions.

A propulsion test was done to evaluate the endurance of the proposed propulsion combination by measuring voltage over time. The motor-propeller setup was mounted to a stand. The throttle was then set to full power to evaluate the static thrust of the motor for takeoff and time the battery took to discharge. Voltage was read at approximately 1 minute. increments using a multi-meter to evaluate the discharge rate of the battery. A new battery was connected to the motor and the throttle was set to reflect cruise power of the airplane. Voltage was again read at 1 minute. increments. The results of the test can be seen in Figure 8.1.

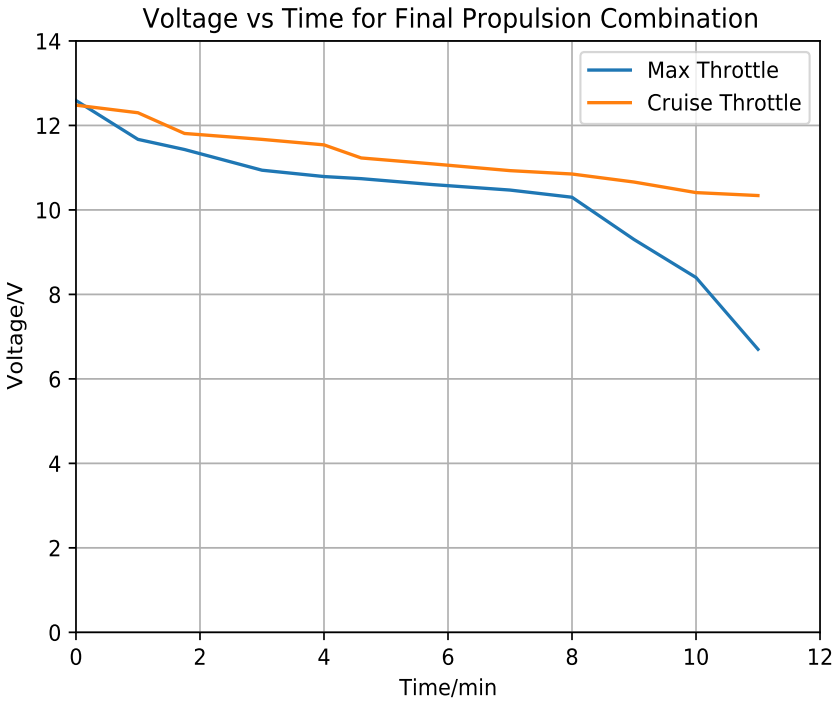

Figure 8.1 – Voltage vs Time for full throttle and cruise throttle of the final propulsion system

The 3S 2200mAh LiPo lasted for over 10 minutes. at cruise speed, meeting the time requirements for Mission 2. At full throttle, the battery steadily discharged for 8 minutes., indicating fast lap completion is possible to increase score for Mission 3. The 2200mAh 3S Lipo, E-Flite Park 480, and 12x7 propeller preformed as expected and verified predictions made in MotoCalc about flight time.

8.3 Takeoff Testing

Due to the mission requirements not placing an emphasis on a short takeoff distance, the takeoff test is primarily used to ensure the airworthiness of the aircraft with a payload. It will also validate that the

placement of the payload is within the CG Tolerance.

8.4 Test Flights

A test flight could not be performed due to material acquisition delay, leading to manufacturing delays.

References

[1] ”2020-21 Design, Build, Fly Rules”, AIAA [online], https://www.aiaa.org/dbf/competition-information/rules-resources.

[2] Hepperle, M., https://www.mh-aerotools.de/airfoils/index.htm

[3] Loftin Jr., L. K., ”Appendix C”, *Quest for Performance: The Evolution of Modern Aircraft*, NASA Scientific and Technical Information Branch, Washington D.C., 1985. https://www.hq.nasa.gov/pao/History/SP-468/cover.htm

[4] Prasuhn, A. L., *Fundamentals of Fluid Mechanics*, Prentice-Hall, 1980.

[5] Raymer, D. P., *Aircraft Design: A Conceptual Approach*, 6th ed., AIAA, 2018.

[6] White, F., *Fluid Mechanics*, McGraw-Hill, New York, 2011, pp. 484-485.